10/12-10-96 JSD

LBNL-38916
UC-2000

ERNEST ORLANDO LAWRENCE
BERKELEY NATIONAL LABORATORY

A Design Study for a Medium-Scale Field Demonstration of the Viscous Barrier Technology

G. Moridis, P. Yen, P. Persoff, S. Finsterle,
P. Williams, L. Myer, and K. Pruess
Earth Sciences Division

September 1996

Available to DOE and DOE Contractors
from the Office of Scientific and Technical Information
P.O. Box 62, Oak Ridge, TN 37831
Prices available from (615) 576-8401

Available to the public from the
National Technical Information Service
U.S. Department of Commerce
5285 Port Royal Road, Springfield, VA 22161

Ernest Orlando Lawrence Berkeley National Laboratory
is an equal opportunity employer.

LBNL-38916
UC-2000

A Design Study For A Medium-Scale Field Demonstration Of The Viscous Barrier Technology

G. Moridis[1], P. Yen[2], P. Persoff[1], S. Finsterle[1], P. Williams[1], L. Myer[1] and K. Pruess[1]

[1]Earth Sciences Division
Lawrence Berkeley National Laboratory
University of California
Berkeley, CA 94720

[2]Bechtel Corporation
San Francisco, CA 94119-3965

September 1996

This work was supported by U.S. Department of Energy, Office of Environmental Management, Office of Technology Development, under Contract No. DE-AC03-76SF00098.

ABSTRACT

This report is the design study for a medium-scale field demonstration of Lawrence Berkeley National Laboratory's new subsurface containment technology for waste isolation dusing a new generation of barrier liquids. The test site is located in central California in a quarry owned by the Los Banos Gravel Company in Los Banos, California, in heterogeneous unsaturated deposits of sand, silt, and gravel typical of many of the arid DOE cleanup sites and particularly analogous to the Hanford site. The goals of the field demonstration are (a) to demonstrate the ability to create a continuous subsurface barrier isolating a medium-scale volume (30 ft long by 30 ft wide by 20 ft deep, i.e. 1/10th to 1/8th the size of a buried tank at the Hanford Reservation) in the subsurface, and (b) to demonstrate the continuity, performance, and integrity of the barrier.

Abstract

TABLE OF CONTENTS

Table of Contents

LIST OF FIGURES

List of Figures

LIST OF TABLES

1. INTRODUCTION

This report is the design study for a medium-scale field demonstration of a new subsurface containment technology for waste isolation developed at the Lawrence Berkeley National Laboratory (LBNL), which uses a new generation of barrier liquids. The test site is located in central California in a quarry owned by the Los Banos Gravel Company in Los Banos, California, in heterogeneous unsaturated deposits of sand, silt, and gravel typical of many of the arid DOE cleanup sites and particularly analogous to the Hanford site.

This effort is part of the project *Containment of Contaminants Through Physical Barriers Formed From Viscous Liquids Emplaced Under Controlled Viscosity Conditions.* Although the project has concentrated on containment in the unsaturated (vadose) zone of the subsurface, the concepts and principles presented here can be easily extended to the saturated zone.

1.1. Conceptual Basis and Project Goals

Lawrence Berkeley National Laboratory (LBNL) staff have developed a subsurface containment technology [*Moridis et al.*, 1993; *Moridis et al.*, 1994; *Persoff et al.*, 1994a; 1994b; 1995; *Finsterle et al.*, 1994a; *Moridis et al.*, 1995*a*] using a new generation of viscosity-sensitive barrier liquids which, when set in porous media, cause the media to exhibit near-zero permeabilities and contain the contamination in the subsurface by entrapping and isolating both the waste source and the plume by a chemically and biologically inert physical barrier.

The current phase of the project involves the second field test of the LBNL viscous barrier technology, and represents a scale-up from the first small-scale field test conducted in January 1995 [*Moridis et al.*, 1995*a*; 1995*b*]. The goals of the current phase of this project are:

(a) To demonstrate the ability to create a continuous subsurface barrier isolating a medium-scale volume (30 ft long by 30 ft wide by 20 ft

deep, i.e. 1/10th to 1/8th the size of a buried tank at the Hanford Reservation) in the subsurface.

(b) To demonstrate the continuity, performance, and integrity of the barrier.

Upon successful completion of the medium-scale field demonstration, the technology will ready for a full-scale field demonstration or application.

1.2. Technology Needs

The development of effective in situ contaminant containment technology is necessitated by the need to prevent further release of contaminants from buried sources and the need to contain existing contaminant plumes. Contaminants from buried wastes or from contaminated soil in the vadose zone can be mobilized and migrate toward previously uncontaminated regions of the aquifer. Contaminant removal is also expensive, very slow, and usually ineffective.

Contaminants cling tenaciously to subsurface materials (especially clays), and traditional physical extraction methods are slow and ineffective. Excavation of contaminated soils and disposal in protected facilities may pose environmental health and safety problems, and is expensive and often impractical.

Despite the obvious need, containment technologies have been largely limited to expensive *brute-force* approaches involving trenching, and cut-off and slurry walls. The applicability of these methods is restricted to cases of lateral movement of contaminants, and their effectiveness is limited due to practical considerations. Currently there is no effective technology to prevent the downward migration of wastes toward deeper and uncontaminated parts of the subsurface.

Subsurface barriers, formed by injection of barrier fluids that gel or solidify in situ, can contain contaminants on-site and control the groundwater flow pattern, thus reducing or eliminating the off-site threat. Moreover, containment is necessary to prevent the spread of mobilized contaminants resulting from application of treatment technologies (e.g., soil flushing, alcohol flooding, surfactant mobilization) that increase the mobility of the contaminants.

1.3. Technology Description

The LBNL viscous barrier technology employs barrier liquids which, when injected into the subsurface, produce nearly-inert impermeable barriers through a very large increase in viscosity. The low-viscosity liquids are injected through multiple injection points in the subsurface and

the intersecting plumes merge and completely surround the contaminant source and/or plume. Once in place, they gel or cure to form a nearly impermeable barrier. The technology can be applied to encapsulate wastes in the subsurface. In applying this technology, however, it is important to match the fluid to the waste and to the soil conditions, and to control the gel time and the emplacement of the fluid to form the barrier [*Moridis et al.*, 1994; *Persoff et al.*, 1994a; 1994b; 1995; *Moridis et al.*, 1995a]

Two general types of barrier liquids have been used. The first is **C**olloidal **Si**lica (CS), i.e. an aqueous suspension of silica microspheres in a stabilizing electrolyte. It has excellent durability characteristics, poses no health hazard, is practically unaffected by filtration, and is chemically and biologically benign. The increase in viscosity of the CS following injection is due to a controlled gelation process induced by the presence of a neutralizing agent or a concentrated salt solution, either of which are added immediately prior to injection at ambient temperatures. The CS has a tendency to interact with the geologic matrix, and therefore, special formulations or techniques are required to minimize or eliminate the impact of such interactions.

The second type belongs to the **P**oly**S**ilo**X**ane (PSX) family, and involves vinyl-terminated silanes with dimethyl side groups. The increase in viscosity in PSX is caused by the cross-linkage of the injected substances and the formation of a matrix of essentially infinite viscosity after the addition of a catalyst through a process akin to vulcanization. The cross-linking process is controlled by the quantities of the catalyst, crosslinker, and (occasionally) retardant added to the PSX prior to injection.

These materials pose no health hazard (have been approved by FDA for food contact), are unaffected by filtration, have low initial viscosity (under 10 cP), are chemically and biologically inert, and have been shown to be effective barrier liquids [*Moridis et al.*, 1995*a*]. Control of the gel time is an essential component of the process because premature or late gelation may result in incomplete coverage of the pore space and thus reduce the effectiveness of the technology.

There are three ways to apply the containment technology. The first, conditions permitting, results in a permanent immobilization of the contaminants by sealing and entombing the entire contaminated region in the subsurface in a *monolith* of inert and impermeable material. This encapsulation represents a radical deviation from the currently predominant approach which either allows the contaminants in a free state and seeks to reduce their rate of migration by reducing the permeability of the porous medium, or attempts to neutralize them through a chemical reaction.

In the second option, an impermeable container (*cage* or *box*) is created to surround and isolate the contaminated area, which can be treated at a later time. Alternatively, such a *cage* could enhance or even make possible remediation techniques (such as soil flushing) which currently face regulatory approval problems due to concerns about contaminants escaping into previously unaffected areas of the subsurface. The design of the medium-level field demonstration discussed in this report is based on the impermeable container approach.

Finally, the third option allows sealing of permeable aquifer zones for the purpose of concentrating the effects of traditional cleanup techniques (such as pump and treat) in inaccessible and less permeable zones, thus increasing the remediation effectiveness.

1.4. Application and Benefits

The LBNL viscous barrier technology can be applied at any site where hazardous wastes (radionuclides, heavy metals, organics, mixed) have contaminated the subsurface environment, and include isolation of ponds and buried tanks, cap and liner repairs at landfills, etc.

The LBNL containment technology offers a number of significant advantages:

- On-site containment and control of the groundwater flow pattern which limits the off-site threat and could supply a long-term solution.
- Site disturbance, if any, is minimal, as no excavation of possibly contaminated soils is required.
- Risk of human exposure is minimized.
- It is applicable to the whole spectrum of wastes and a wide variety of sites.
- It enables the complete isolation of the affected area from the regional groundwater flow by providing barriers to both horizontal and vertical flow (the only technology currently capable of providing horizontal barriers (bottoms) in containment systems).
- It is usually cheaper and more effective than conventional (baseline) methods.
- The effectiveness of traditional clean-up techniques can be enhanced by allowing natural degradation and bioremediation to occur without risk of contaminant migration.
- Additionally, more intensive remediation technologies (such as soil washing, alcohol flooding, etc.) are possible without the risk of mobilization of the contaminants.

2. PREPARATORY WORK

In this section we discuss the preparatory supporting work that provided the necessary information for the design planning of the medium-level field demonstration of the LBNL barrier fluid technology. This work included

- the identification and characterization of promising materials,
- the evaluation of their containment potential by means of laboratory and pilot-scale experiments,
- the development of predictive capabilities for the study of a number of alternative injection scenarios through numerical simulation,
- the interactions with industry, academia, and regulatory agencies, as well as
- the design and successful execution of the first-level field demonstration of the LBNL containment technology.

The discussion in this section is brief and limited in scope, and is intended to provide headlines that trace the information flowchart and overall project approach for the understanding of the activities that led to current phase of the project, i.e. the design and preparation for the second (medium-level) field test. Where warranted, the most important of these activities are discussed in far more detail in subsequent sections of this report. Additional information on the remainder of these activities can be found in a number of related reports.

2.1. Studies of Materials and Processes

(a) We completed a wide search for fluids with desired properties

(b) We identified three types of promising substances for evaluation as barrier fluids: Colloidal Silica (CS), Polysiloxanes (PSX), and Polybutenes (PB). From the beginning of FY 1994 work has concentrated in Colloidal Silica and Polysiloxanes due to budget and time restrictions, as well as concerns about the potential effects of soil preheating on the contents of buried tanks at the Hanford site, the initially intended application site of this technology.

(c) We investigated a number of possible ways to use these materials: pure, in suspensions, diluted in compatible products, etc., and determined that optimum results were obtained with pure substances.

(d) We completed the analysis of the rheological and wettability properties of the barrier fluids. We determined the complex viscosity behavior of the barrier fluids, and developed their gel time curves. The wettability studies demonstrated some unique properties, the most noticeable of which was that PSX has a 180° contact angle with both water-wet and oil-wet surfaces, and as such can wet both with the same ease. The implication of this behavior is that PSX can coat and isolate soil grains covered with organic contaminants.

(e) We conducted a series of laboratory studies of barrier fluid flow and emplacement in porous media, and determined that all three types of liquids are effective in sealing porous media.

(f) We identified the dominant mechanisms in Colloidal Silica gelation in porous media. We determined that in addition to the mechanical effect of pore sealing CS has the additional advantage of being able to immobilize heavy metals by incorporating them into the gel structure. We also determined that the soil chemistry may have a pronounced effect on the gel times.

(g) We developed alternative processes to alleviate possible effects of the soil chemistry on the CS gel time, and ways to control the gel time and the texture of the gels. We determined the need and designed protocols for the sequential injection of CS, and demonstrated that soil hydraulic conductivities were reduced from 10^{-4} m/sec to less than 10^{-10} m/sec after two injections.

(h) We developed processes to control the viscosity and gel time of Polysiloxanes. We determined that the PSX crosslinkage times are far less sensitive to the soil chemistry than CS, and demonstrated that hydraulic conductivities could be reduced from 10^{-4} m/sec to 10^{-12} m/sec after a single injection.

(i) In collaboration with the manufacturers, we had new CS and PSX formulations developed to meet barrier fluid requirements. The new CS formulation developed for LBNL is unaffected by the soil chemistry, and the new PSX formulation has a low initial viscosity. Both the new CS and PSX products have low enough viscosities to allow injection using regular, currently available grout injection equipment without any alteration.

(j) We conducted a series of laboratory tests designed to investigate the barrier performance of CS and PSX at all length scales of interest, from sub-millimeter (pore micromodels) to one-dimensional experiments (column studies) to two-dimensional studies in tanks

(ranging in size from 0.3 m × 0.3 m × 0.3 m to 2.1 m × 1.8 m × 0.15 m).

(k) We conducted preliminary waste compatibility tests, and concluded that both CS and PSX are not significantly affected by the types of wastes contained in the buried tanks at Hanford.

2.2. Predictive Capabilities

(a) We expanded [*Finsterle et al.*, 1994b] and modified TOUGH2 [*Pruess*, 1991], the LBNL general code for the simulation of mass and heat flow and transport in the subsurface, to predict the flow and behavior of gelling/cross-linking fluids and evaluate the performance of barrier liquids.

(b) We then used the expanded TOUGH2 to design the laboratory experiments (one- and two-dimensional) of barrier fluid injection, and conduct a sensitivity analysis of the relevant parameters. A significant portion of the design work discussed in this report is based on TOUGH2 simulations.

2.3. Interactions with Industry, Academia, and Regulatory Agencies

(a) We developed an agreement with Bechtel Corporation (a large diversified engineering firm with extensive expertise and background in soil grouting in a variety of sensitive applications) to collaborate in the area of barrier fluid emplacement. Working with Bechtel, a work-plan for a first-level injection test and a field demonstration at Hanford have been finalized.

(b) We signed a confidentiality agreement with Dow Corning, the manufacturer of PSX, and developed a CRADA proposal for joint work on a new generation of barrier fluids. As a result of this collaboration, Dow Corning made available to the project the new low-viscosity PSX used in the experiments.

(c) We developed a collaborative agreement with DuPont for the development of CS containment technology. DuPont has contamination problems at a number of manufacturing sites, and is also the manufacturer of a CS family of materials. As a part of their containment effort, DuPont conducted an early field test. The results of the DuPont work became available to LBL through a confidentiality agreement (signed in Feb. 1994) for review and analysis, and offered a valuable insight into potential problems related to the field application of CS-based barriers.

(d) We developed collaborations with Texas A&M University and the University of California at Berkeley. Texas A&M University helped evaluate the performance of barrier fluids in large two-dimensional laboratory experiments using their unique dual-gamma attenuation facility. This is the most accurate and most powerful such facility in the world, and allows the non-destructive determination of the barrier fluid saturation in the soil. UC Berkeley (Chemical Engineering Department) was involved in the detailed rheological study of the barrier fluids using their specialized equipment.

(e) We developed agreements for possible applications of the barrier technology at a number of military bases: McClellan Air Force Base (AFB), Mather AFB, and Hill AFB. Interest has been shown by the U.S. EPA, the Dept. of the Navy (Naval Air Weapons Station, Hunters Point Shipyard), the Dept. of the Army, the Lawrence Livermore National Laboratory, as well as the State of California (Regional Water Quality Control Board).

(f) Both the first-level injection test and the medium-scale field demonstration received a Categorical Exclusion from NEPA regulations due to the environmentally benign nature of the barrier fluids. The California Department of Toxic Substances gave its consent to this field test.

2.4. The First-Level Field Demonstration

In the following subsections, various aspects of the first-level field demonstration which occurred in January 1995 are described. These include the objectives of the demonstration, the necessary preparatory work, a site description, specification of the barrier liquids, and the four stages in executing the demonstration: (a) well drilling and permeability measurements, (b) barrier fluid injection, (c) grouted bulb (plume) excavation and sample recovery, and (d) laboratory investigations of grouted samples. A detailed discussion of the first-level field demonstration can be found in *Moridis et al.* [1995a].

2.4.1. Objectives of the First-Level Field Demonstration

The objectives of the first-level field demonstration were to demonstrate the ability to:

- inject colloidal silica and polysiloxane using standard permeation grouting equipment,
- track the grout fluid movement using tiltmeter measurements of ground surface deformation,
- control the grout fluid gel time under *in situ* chemical conditions,
- create a uniform grout plume in very heterogeneous matrices including cobbles, gravels, sands, silts and clays,

- create intersecting/merging plumes of grout, and
- decrease the permeability of the grouted soils.

The demonstration was not intended to prove the creation of continuous and/or impermeable barriers. Such an effort would be significantly larger in scope and involve merging and overlapping the injected barrier liquid plumes, as well as multiple injections.

2.4.2. Preparatory Work for the First-Level Field Demonstration

The Underground Storage Tank Integrated Demonstration (UST ID) at Hanford, Washington, was identified as the area of first application of this technology. We had a number of meetings with PNL, Westinghouse Hanford Co., and DOE officials to discuss the corresponding field application of the technology.

We developed a design package for the application of the viscous barrier technology at the UST ID at the Hanford site. Using TOUGH2, we designed a first-level injection test to be conducted at the Hanford site. In addition, we completed a preliminary evaluation of geophysical techniques for monitoring barrier performance and emplacement [*Moridis et al.*, 1996]. However, due to institutional problems, it was not possible to conduct the test at Hanford within a desired budget and time frame.

It became evident in May 1994 that conducting the first field test at the Hanford site could entail significant delays and higher costs (substantially exceeding the project budget). Several alternative sites were evaluated, from which we identified a local site in California with a subsurface geology similar to that at Hanford. After obtaining permission from the owner and the regulators to conduct the first-level test there, a Host Site Agreement was signed, and a Categorical Exclusion from NEPA and EPA regulations was obtained for a field test at that site.

2.4.3. The Site

The test site is located in central California in a quarry owned by the Los Banos Gravel Company. The quarry is situated along the western flank of the San Joaquin Valley, adjacent to the eastern margin of the central California Coast Ranges. The quarry exploits river gravels in a 100 km^2 alluvial fan generated by Los Banos Creek at the foot of the California Coast Range. The deposits exposed at the quarry are primarily coarse sands and gravels, deposited on a distributary lobe of Los Banos Creek adjacent to its present channel. They are internally heterogeneous, with discontinuous and lenticular coarser and finer strata, and occasional lenses of well-sorted cross-bedded sands.

Large gravel and cobble clasts are commonly set in the sandy matrix, and range between 1 and 10 cm. The matrix is predominantly coarse sand (0.5-1 mm), and comprises varicolored lithic fragments. Induration, where present, is caused by infiltration (illuviation) of clay into

pores between sand grains; a fine film of yellow-brown clay can be seen binding the sandy matrix in most samples.

2.4.4. The Barrier Liquids

The barrier fluids selected for injection included one type of PSX (hereafter referred to as PSX-10) and one type of CS (Nyacol DP5110). In preliminary experiments, other variants of PSX and CS products were also tested. All the barrier fluids tested are environmentally benign and carry no warning label requirements.

Nyacol DP5110 is a CS in which silica on the particle surfaces has been partly replaced by alumina; its solid content is 30 wt.% and its pH is 6.5. A technical grade aqueous solution of $CaCl_2$ was used to promote gelation for the final tests and the field demonstration. The concentration of the solution was nominally 35 wt.% (4 mol/L) $CaCl_2$.

PSX-10 is a polydimethylsiloxane, divinyl terminated to provide active sites for cross linking. It is formulated with a cross linker that reacts with the vinyl terminations in the presence of small concentrations of a platinum-based organometallic catalyst. The polydimethylsiloxane and crosslinker are delivered already mixed, but unreacted. A platinum based catalyst is added at the level necessary to achieve the desired gel-time.

2.4.5. Well Drilling and Permeability Measurements

Four injection and four observation wells were drilled. The injection wells were drilled to a depth of 16 ft, while the observation wells were drilled to depths ranging between 12 and 20 ft. Following well completion, all the wells were fitted with appropriate tubing, and probes were punched through the bottom of the wells for air permeability measurements.

Air permeability measurements included static single point permeameter tests using constant head air injection tests, and a new dual probe dynamic pressure technique developed at LBNL for measurement of air permeability between wells [*Garbesi*, 1994]. The latter uses a sinusoidally varying pressure with a mean near-atmospheric pressure at the injection well. Pressure responses are continuously monitored at several observation wells. The single point permeameter technique provides information on the permeability immediately surrounding each well, while the dual probe technique provides information on the permeability between wells.

The static permeability measurements, conducted in all eight wells, indicated permeabilities ranging from a high of 10^{-10} m^2 to a low of 3.6×10^{-13} m^2. Injections into holes AP1, CS1, and CS2 using the new dual probe dynamic pressure technique, yielded inter-hole permeabilities between 3.5×10^{-9} m^2 and 10^{-11} m^2. The apparent lack of agreement is due to conceptual differences between the two approaches: the static technique in essence measures the permeability at the point of injection, whereas the

dynamic technique measures the mean permeability between a source and a receptor well along paths that are not necessarily the shortest.

After completing the air permeability tests, all observation wells were plugged to prevent barrier liquids from flowing into the observation wells and bypassing the area to be grouted. The bottoms of the injection wells were also plugged.

2.4.6. Barrier Fluid Injection

The barrier liquids were injected through 3 ports in each well (at depths of 10, 12, and 14 ft) using the tube-à-manchette technique. Approximately 400 gallons of CS grout were injected into two wells, CS1 and CS2. About 120 gallons of PSX-10 were injected into a single well, PS1. The smaller scale of the PSX-10 injection test was dictated by budget considerations, as it is still a developmental product and economies of scale in its production have not yet been realized.

The barrier liquids (CS and $CaCl_2$ brine, PSX-10 and catalyst) were premixed at the surface using the agitators of the mixing tank and the recirculation equipment of the grouting system. For the CS injection, food-color dye was added to enhance its visibility during subsequent excavation of the site. Green dye was added to the batches injected into CS1, and purple dye into the CS2 batches. The same quantity of barrier fluid (66 gallons for CS, 40 gallons for PSX-10) was injected at each depth.

Standard chemical grouting equipment was used for delivering the barrier fluids to the hole. The procedure for injection followed those typically used in *tube-à-manchette* grouting. The injection sequence was carried out in order to maximize complete permeation of the soil in the vicinity of the wells. Thus injection began at the lowest port (14 ft), followed by injection through the uppermost port (10 ft) and, finally, injection through the intermediate depth port (12 ft).

The barrier fluids were injected without any significant rise in pressure (which would have indicated premature gelling). During injection the volume of injected grout and injection pressure were monitored. Average values of injectivity, a measure of the apparent permeability at each injection port, decreased with depth with values at the 14 ft depth an order of magnitude or more lower than those at shallower depths.

Eight tilt meters were installed at the injection site. Tiltmeters measure the angle of deviation of the land surface from the vertical axis. Because the deformation detected by tiltmeters is minuscule (nano- to micro-radians), LBNL staff decided to apply this technology to track the swelling and uplift at the earth's surface due to the intrusion of the barrier liquids. The tiltmeter array recorded ground movement every 60 seconds throughout the test, and was able to detect movement of the injected fluids.

Deducing the movement of fluids through the subsurface from surface tilt requires the solution of an *inverse* problem, which cannot presently be conducted in the field in real-time, although such is anticipated with the rapid advancement of computer technology.

2.4.7. Excavation and Visual Inspection

The excavation of the grouted plumes was facilitated by the proximity of the wells to the exposed face of the quarry (20 ft) and the use of heavy earth moving equipment. The ground was excavated to a depth of up to 21 ft. Both CS and PSX-10 had satisfactorily gelled/crosslinked in the subsurface. Despite the extreme soil heterogeneity, both the CS and the PSX-10 created fairly uniform plumes, indicating that the potential problem of flow along preferential pathways of high permeability (such as a gravel bed overlying a tight silty or clayey zone) can be overcome.

The CS grouted and sealed fractures and large pores in the clays. In open zones (such as gravels with cm-sized pores) it did not fully saturate the voids, but appeared to have sealed access to them. CS did not impart substantial structural strength to the matrix, but permitted vertical sections of the matrix (with the exception of very loose and friable materials) to stand.

PSX-10 was singularly successful in grouting the extremely heterogeneous subsurface at the site. PSX-10 created an almost symmetric plume, grouting and sealing gravels, cobbles, sands, silts, and clays. PSX-10 filled and sealed large pores and fractures, as well as accessible small pores in the vicinity of these pores/fractures. In extremely large voids in open zones, it coated the individual rocks in the gravel and sealed access to and egress from these zones. PSX-10 also invaded clays and silts, which is unusual. The mechanism through which this penetration is achieved has not been determined, but is under investigation.

PSX-10 is relatively easy to identify in the subsurface. Unlike CS, PSX-10 imparted structural strength and elasticity to the grouted soil volume, and gave sufficient strength to incoherent gravels to permit vertical walls to stand. It fully penetrated clean sands, which resisted disaggregation due to its considerable elasticity.

2.4.8. Post-Excavation Analyses

The grouted plumes were excavated primarily to determine the volumetric extent of the grouted zone. LBNL staff also took advantage of the excavation to recover boulder-size chunks of grouted sand from which smaller samples could be taken for permeability measurement in the laboratory. After excavation, grab samples of ungrouted matrix were taken at various depths from locations adjacent to the grouted bulbs. Both moisture content and material gradational analyses were performed on these samples.

The permeabilities of the grouted sand samples were measured using a flexible wall permeameter. Samples from the field were cored or carved from the boulder-sized chunks for insertion into the permeameter. Coring using a soil-sampling tube was possible only with a material containing no pebbles. The extreme heterogeneity of the formation at the Los Banos site

made it difficult to sample and make permeability measurements. Hence, the number of field samples subjected to permeability testing was limited.

Because the field samples are expected to have the greatest amount of ungrouted voids, multiple injections will be required to achieve permeability reductions sufficient for barrier performance. This goal was not pursued in the first-level field injection, as the reduction of permeability to a near-zero level was not among the objectives of this field demonstration for the reasons discussed earlier.

In the case of field-grouted sand and pebbles, the observed hydraulic conductivities reflect incomplete saturation of the pore space. Damage to samples during recovery, transport, storage and trimming to fit the apparatus could also have contributed to increases in hydraulic conductivity. Similar values were observed whether CS or PSX-10 grout was used, but this may not mean anything since they were different samples from different locations and with different soil textures. Partial saturation of pore space is also suggested by the observation of the larger than expected plumes. This supports the view that grout desaturation occurred due to plume spreading. LBNL's plume emplacement model predicts that this phenomenon will always occur in the vadose zone.

The grouted Los Banos material is 2 orders of magnitude less permeable than the ungrouted sand fraction of these materials. The sand fraction is less permeable than the actual soil due to its finer texture. Compared to the field measurement of air permeability, these samples indicate a permeability reduction by 3 to 4 orders of magnitude. In that respect, the results are very encouraging.

Data from the tiltmeter measurements were inverted in order to relate the tiltmeter measurements to the shape and extent of the injected grout plume. Based on the inversion results, the ground motion due to injection could be predicted. The peak vertical displacement of the land surface due to injection of CS was found to be 0.18 micrometers. The preliminary work suggests that tilt measurements can be used to monitor subsurface injections. However, further refinement of the technique is required for future application.

In conclusion, LBNL staff believe that the first field test was an unqualified success, and that the objectives were achieved.

3. THE BARRIER LIQUIDS

The barrier liquids to be used in the medium-scale field demonstration are the same as in the first-level field test (see subsection 2.4.4). As discussed earlier, our effort focused on two barrier liquids: **C**olloidal **S**ilica (CS) and **P**oly**S**ilo**X**ane (PSX).

CS and PSX may vary substantially in the effect of the soil chemistry on their gelling and crosslinkage performance respectively. PSX exhibits slight and/or controllable effect of the soil chemistry on crosslinkage. Although such compensation was not possible in the case of commercially available CS products (which demonstrated a drastic acceleration of gelation due to soil chemistry [*Moridis et al.*, 1995a), new CS variants made to LBNL's specifications by the manufacturer alleviated the problem.

3.1. Design Parameters, Issues, and Implications

(a) The materials to be used in the medium-scale field demonstration are the same used in the first-level field test in January 1995, i.e. CS (Nyakol 5110) and PSX (PSX-10).

(b) The initial viscosity of CS and PSX is 5 and 10 cP, respectively, which allows easy injection with conventional equipment.

(c) Based on our previous experience with the Los Banos soils, possible soil effects on the CS gelation and PSX crosslinkage can be easily controlled.

(d) The CS gelation and the PSX-10 crosslinkage may be affected by
- the magnitude of the liquid and surface (air) temperature,
- diurnal and daily variations in air temperature, and
- the difference between liquid and subsurface temperatures.

(e) The design gel/crosslinkage time for the CS and PSX is 2-2.5 hrs.

(f) Variability between batches of the barrier liquids may be observed. Testing of each batch prior to injection is necessary.

(g) The barrier liquid selection will be dicated by budget considerations. Ideally, the demonstration will include both a CS and a PSX containment system. If the available budget is insufficient, a combination of CS and PSX (with PSX coating a CS core) could be used. If the budget cannot support the dual-material option, then CS will be the barrier liquid of choice due to its considerably lower cost.

3.2. Background Information

The barrier fluids used in this work represent a new generation of chemical grouts. Chemical grouts are generally prepared by mixing two or more liquids, and the resulting mixture changes from a liquid to a *pseudo-solid* state during some period of time. We refer to the final state as *pseudo-solid* because it is amorphous and lacks the crystalline structure invariably associated with real solids. In that respect, the gelled materials can be considered liquids with infinite viscosity. The grout can be injected only until a certain time, referred to as gel-time, has elapsed. The process of *solidification*, caused by gelling or crosslinking, begins as soon as the ingredients are mixed.

For operational simplicity, and to allow grout emplacement using commonly available equipment, the ingredients of the barrier fluids in the field test injections were not mixed in-line but were rather premixed as a batch. This dictates a gel-time long enough to accomodate the time requirements for mixing and injection, while accounting for potentially accelerating effects of the soil chemistry on the grout. As will be discussed later, formulas for both materials were developed to meet a design criterion of a minimum of a 2-hr gel-time. That is, the barrier liquids were to remain sufficiently mobile to allow injection for at least two hours after mixing.

Our effort concentrates on the creation of barriers in the unsaturated zone of the subsurface, which imposes special requirements on the gel-time of the barrier liquids. Unlike the saturated zone, it is not possible to exert hydraulic control on the emplacement and flow of barrier fluids in the unsaturated zone. After injection, the forces acting on the plume of the barrier liquid are gravity and capillarity, both of which result in the redistribution of the grout: gravity will cause the downward migration of the plume as well as spreading by dispersion, while capillarity will tend to spread the plume. Our numerical model accounts for all these phenomena.

The net effect of these forces acting in concert is the reduction of the saturation of the barrier liquid (i.e. the portion of the pore space occupied by the grout) which results in a permeability reduction smaller than optimal. The implication of these practical considerations is that the gel-time of the barrier liquids has to be within a certain time window: long enough to allow comfortable emplacement and prevention of premature gelling (with a resulting reduced coverage), but sufficiently short to prevent excessive redistribution and reduction in the soil saturation.

3.4. Colloidal Silica (CS)

The CS variant to be used in this demonstration is Nyacol DP5110 (PQ Corporation, Valley Forge, PA). Nyacol DP5110 is a CS in which silica on the particle surface has been partly replaced by alumina; its solid content is 30% and its pH is 6.5. Gellation of DP5110 will be induced by using a $CaCl_2$ electrolyte solution.

In traditional base-stabilized CS systems, particle charge induced by high pH is temporary in the sense that it can be increased, decreased, removed, or even reversed according to the pH value. In the new DP5110 formulation (made available to the project by the manufacturer in July of 1994), the CS is stabilized by a permanent particle charge produced by isomorphic replacement of Si by Al on the particle surface (**Figure 3.1**). In the resulting **C**olloidal **A**lumina **S**ilica (CAS) the charge is not pH dependent and it is even more environmentally benign because it is stable at a near-neutral pH of 6.5.

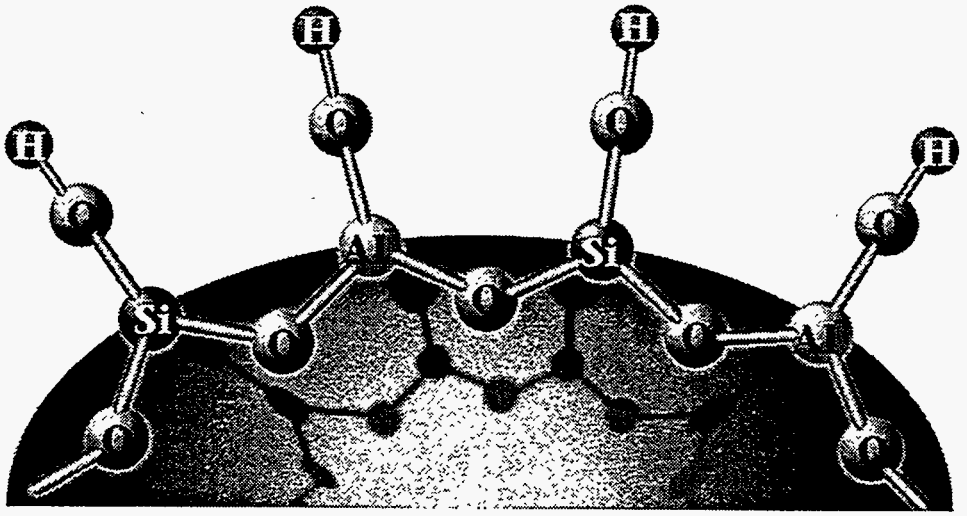

Figure 3.1. Isomorphic substitution of Si by Al on the CS surface in the DP5110 formulation

Gel-time jar tests on Nyacol DP5110, the CAS developmental product, appear in **Figure 3.2**. CAS gelled with NaCl brine has gel-times that are unacceptably long for the majority of applications, but practical gel-times (1-10 hrs) are achieved with a $CaCl_2$ gelling agent. By using a grout containing Ca^{2+} ions, the release of Ca^{2+} from clays in the soil by ion exchange ceases to be a problem. The principal advantage of using DP5110 is that its gelling rate is relatively (but not totally) unaffected by soil.

Figure 3.2 shows gel-time jar tests with and without soil. No acceleration is evident in the initial tests with a soil-CAS ratio of 10 g : 24 mL, but measurable acceleration may be observed with higher soil to CS ratios [*Moridis et al.*, 1995*a*]. The target gel-time is 2-2.5 hours, which can be achieved by using a 0.3-0.4 M $CaCl_2$ solution (**Figure 3.2**).

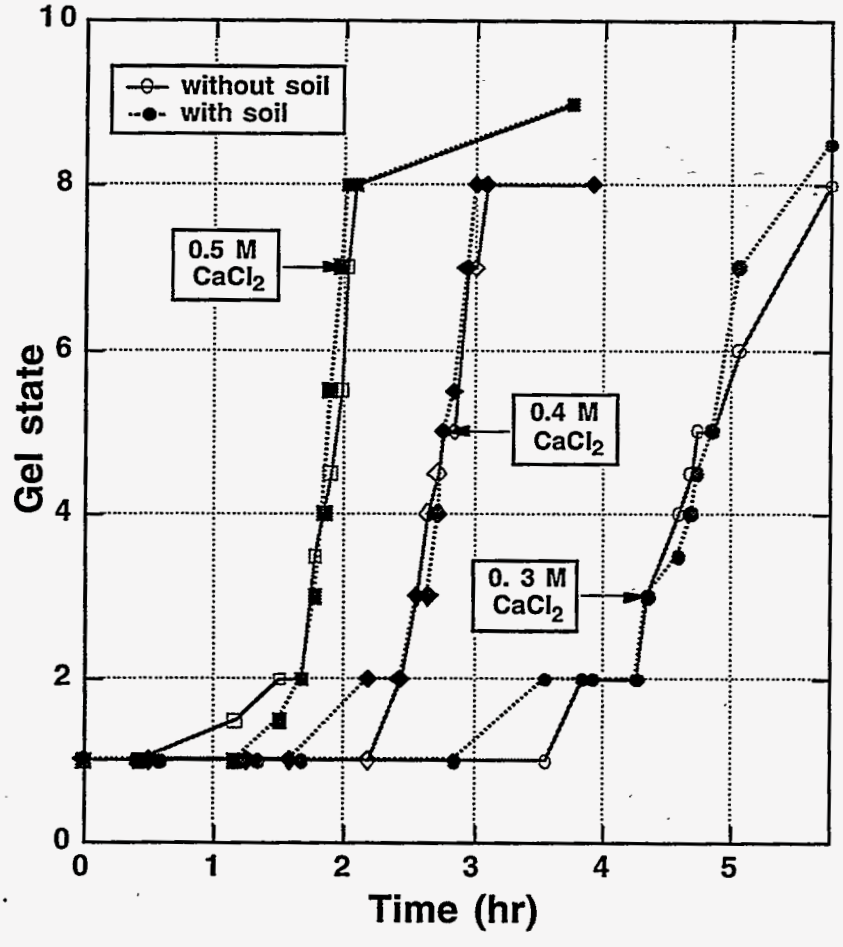

Figure 3.2. Effect of addition of Los Banos soil on the gel-time of Nyacol DP5110.

Injection tests into columns (**Figure 3.3**) confirmed that this grout formula could be injected into the soil without premature gelling. Results of viscosity measurements of the CAS DP5110 grout are presented in **Figure 3.4**. These data (appropriately scaled to account for temperature and CAS variability effects) were used in the numerical simulation for the design of the field test.

During the first-level field injection [*Moridis et al.*, 1995a; 1995b], batches were sampled to observe the gelling of the grout. It was soon apparent that the batches were gelling more slowly than expected. This was attributed to (a) batch variability, and (b) the low ambient temperature, which at about 5 °C was significantly lower than the laboratory temperature of 20 °C at which all measurements and gel-tests had been made. Similar problems could occur during the medium-scale field-test, a possibility which necessitates testing of each batch and accounting for temperature effects.

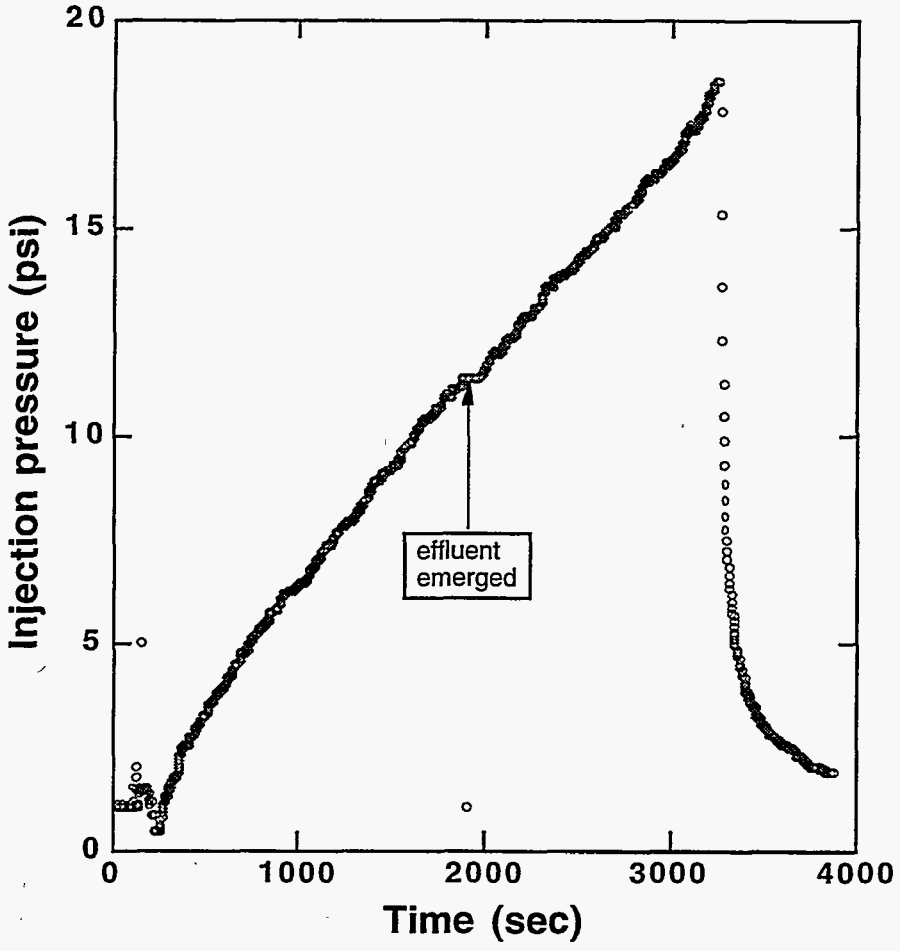

Figure 3.3. Column injection test of CAS Nyacol DP5110 into GFA sand. Both the colloid and brine were the same materials as used in the field test.

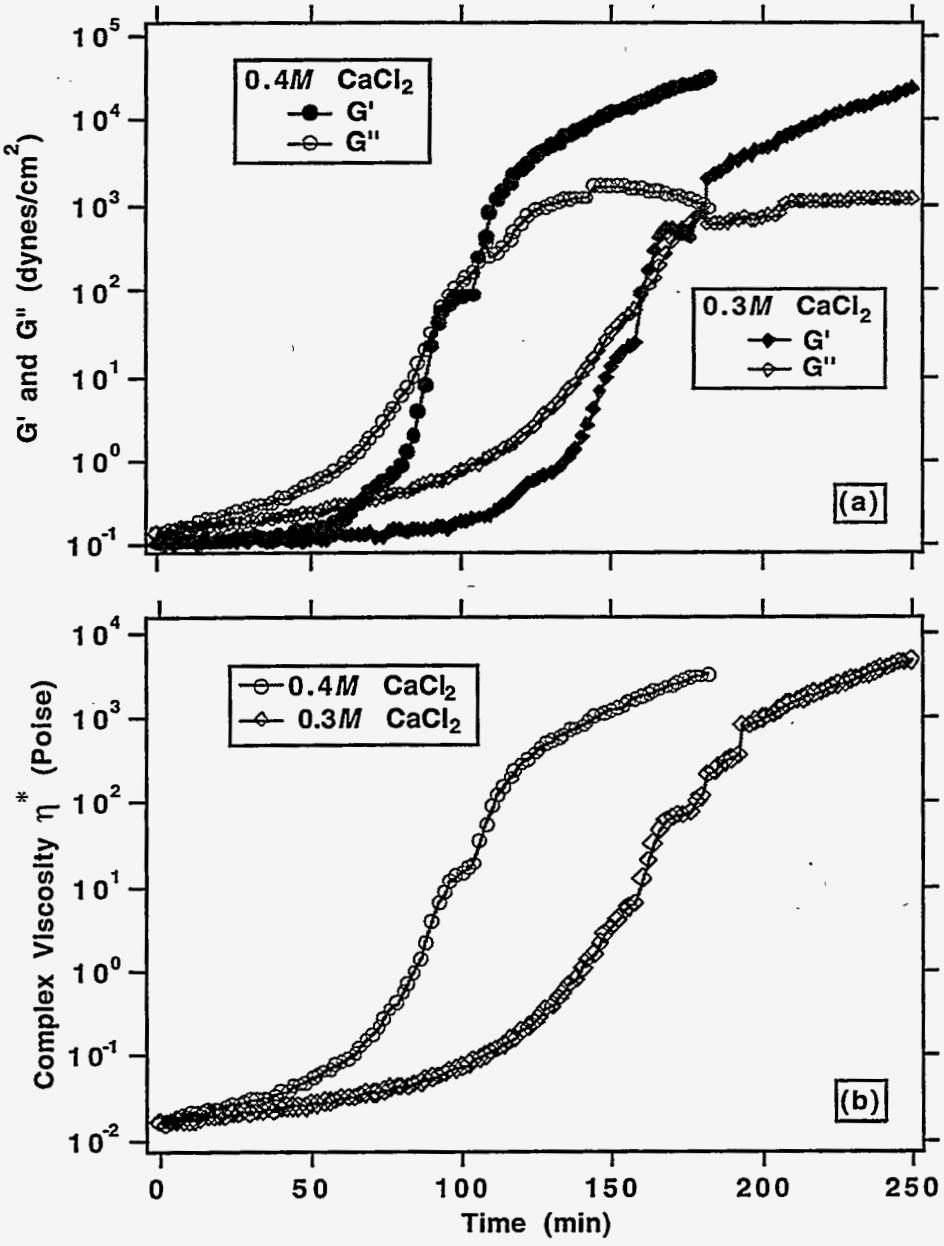

Figure 3.4. Rheological analysis of CAS Nyacol DP5110: (a) viscous and elastic moduli, and (b) complex viscosity during gelling with 0.3 and 0.4 M $CaCl_2$ brines (Rheometrics dynamic spectrometer data).

3.5. Polysiloxane (PSX-10)

The polysiloxane 2-7154-PSX-10 used in our field test was developed by Dow Corning especially for this application. The final "10" in the designation refers to the viscosity, which at 10 cP is low enough to allow penetration into otherwise ungroutable fine soils and use of conventional injection equipment without any modification. The PSX-10 grout system consists of five components:

(1) A di-vinyl-terminated polydimethylsiloxane polymer:

$$H_2C{=}CH\text{-}Si(CH_3)_2\text{-}O\text{-}[Si(CH_3)_2\text{-}O]_n\text{-}Si(CH_3)_2\text{-}CH{=}CH_2$$

(2) A di-hydrogen-terminated polydimethylsiloxane polymer:

$$H\text{-}Si(CH_3)_2\text{-}O\text{-}Si(CH_3)_2\text{-}O]_n\text{-}Si(CH_3)_2\text{-}H$$

The distribution of the number n controls the viscosity. The first and second C atoms in the vinyl group are termed the α and β carbons.

(3) A cyclic polyvinylmethylsiloxane crosslinker

$$[\text{-}Si(CH_3)(CH{=}C_2H)\text{-}O\text{-}]_m$$

in which the number of units m is between 4 and 6.

(4) The catalyst.

(5) An inhibitor to prevent rapid crosslinking to prevent rapid crosslinking when the catalyst is first added. Depending on the length of the desired gel-time, additional amounts of inhibitor may be added.

Ingredients 3, 4, and 5 are present in very small amounts. Cross-linking occurs when reactions occur between the H terminations and the cyclic or terminal vinyl groups. The double bond of the vinyl group is broken, the terminal H goes to the β carbon and a bond is formed between the α carbon and the Si that loses its terminal H. Cross-linking reactions therefore can link several hydrogen-terminated chains to a single cyclic molecule, forming a complex polymer network.

As the polymer crosslinks, it changes from a Newtonian fluid to a viscoelastic fluid, to an elastic solid. We will use the term *gelling* to describe this process although the mechanism is different from the gelling of CS described previously.

Viscosity data measured with the Rheometrics dynamic spectrometer for PSX-10 during gelling with various catalyst concentrations are shown in **Figures 3.5** and **3.6**.

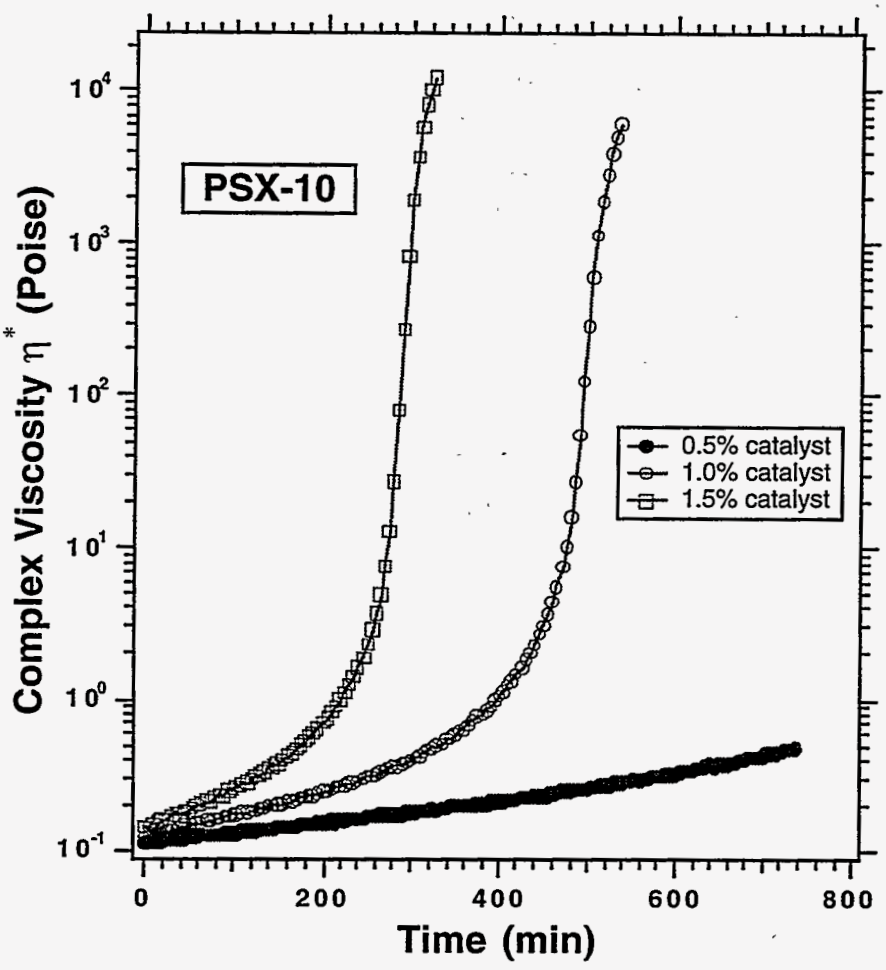

Figure 3.5. Complex viscosity of PSX-10 during gelling, with catalyst concentration ranging from 1 to 2 %.

Gel-time curves were also developed for PSX-10 at various temperatures, and catalyst concentrations, with and without Hanford soil. Data are shown in **Figures 3.6** and **3.7** for gel-time jar tests at 20 and 38 ^{o}C, with catalyst concentrations ranging from 1 to 2 % by weight. The effect of temperature was studied because of the range of the expected temperatures that might be experienced during field trials. **Figure 3.8** shows results of a column test injection of PSX-10 with 1% catalyst into GFA soil.

From these figures it is obvious that the main means to control the gel-time is by varying the amount of catalyst. However, there is a lower bound to the catalyst amount, below which gel formation does not occur. When longer gel-times are desired, varying the amount of the retardant may offer an additional means of control (**Table 3.1**).

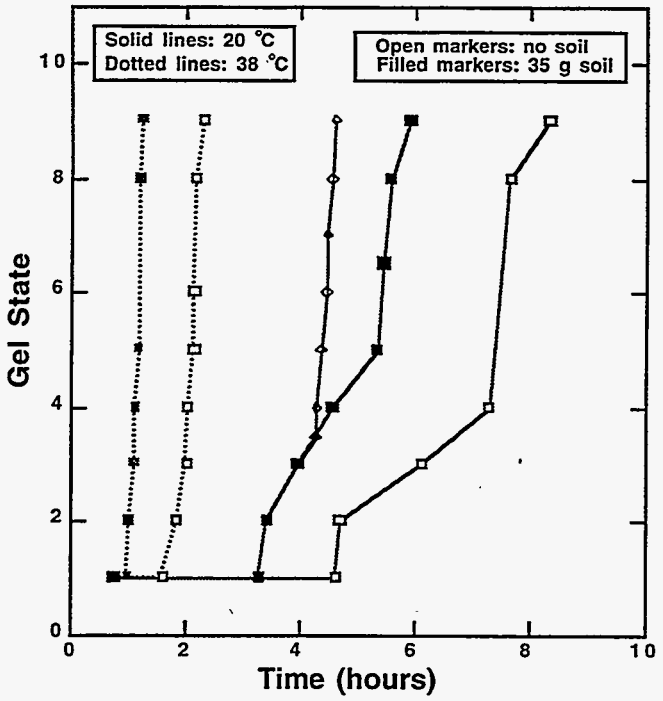

Figure 3.6. Gel-time curves for PSX-10 at 20 and 38 °C, with and without soil, 1.5% catalyst.

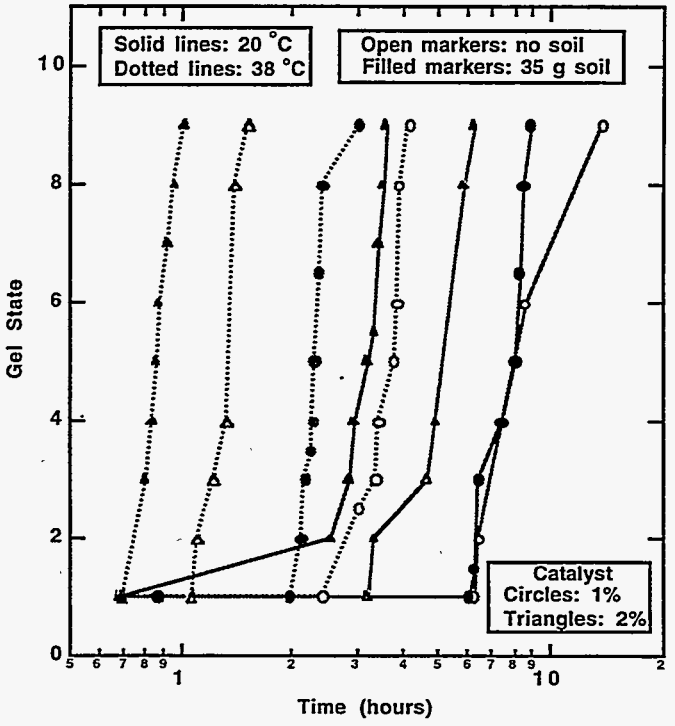

Figure 3.7. Gel-time curves for PSX-10 at 20 and 38 °C, with and without soil, 1 and 2% catalyst.

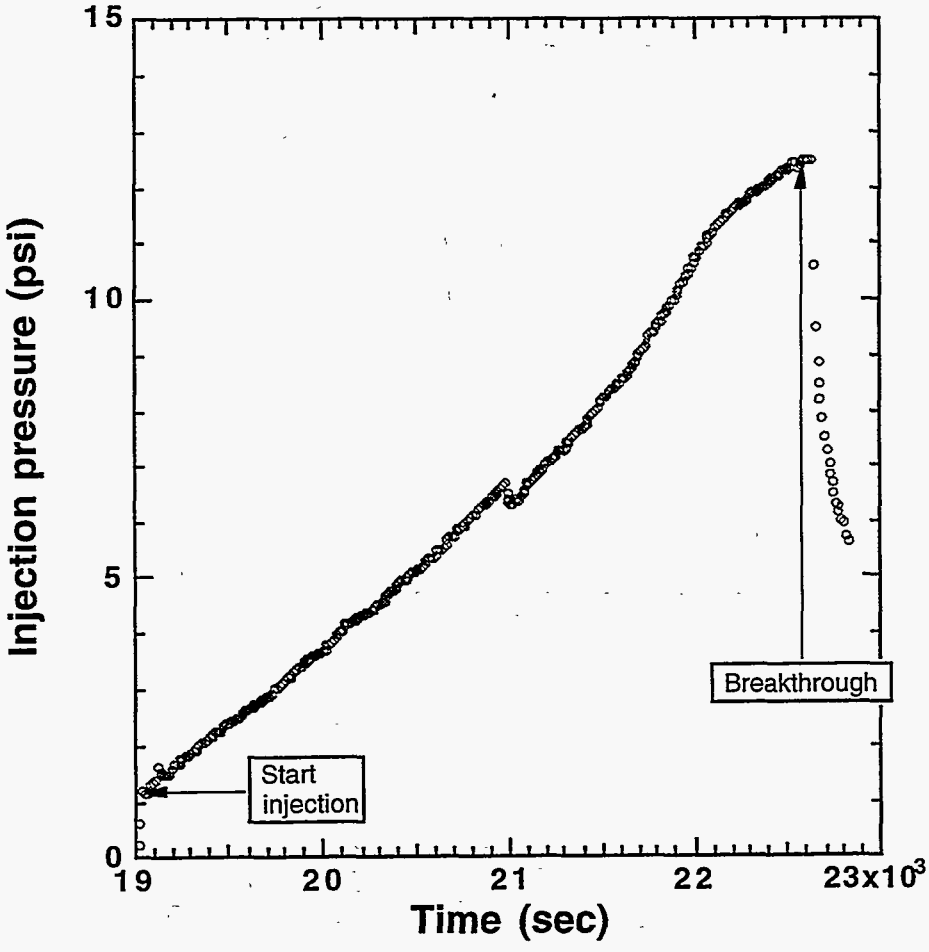

Figure 3.8. Column injection test of PSX-10 with 1% catalyst into Los Banos soil.

After studying the effects of the retardant and evaluating our options, we decided that the 2-hr gel-times needed for our field test could be easily accommodated by varying only the catalyst. Soil seems to have a slight accelerating effect on the gelling of PSX, but the degree of acceleration can be easily compensated for by adjusting the catalyst concentration.

After the field injection, we conducted additional tests to determine the effect of water on the gelling of PSX, and extended the temperature range downward. Data for jar tests using 1.25% catalyst at 4, 20, and 43 °C are presented in **Figure 3.9.** Blanks with no catalyst were also tested.

Samples with tap water were shaken vigorously by hand for about 30 seconds to provide mixing. Two emulsion layers were formed: water-in-PSX on top and PSX-in-water at the bottom. In samples which did not contain catalyst (blanks), the emulsions broke within 3 minutes. In samples with catalyst the bottom layer took longer to clear (from 30 minutes to 1

hour), and the top layer never broke. Instead, the layer crosslinked to form a solid mass incorporating emulsified water.

Figure 3.9 shows that the samples without water gelled slower than expected, while the samples with water had gel-times consistent with expectations from previous jar tests. The reason for slow gelling without water is not known, but it may have been caused by catalyst poisoning.

As with the colloidal silica, temperature during the field demonstration is expected to have an effect on crosslinking. Observation of grout samples in jars during the first field demonstration suggested that the grout remained mobile longer than 5 hrs, i.e. double the target (design) gel-time [*Moridis et al.*, 1995a]. This may have an effect on the degree of saturation of the treated volume, as longer gel-times may result in greater spreading of the grout in the subsurface.

Table 3.1. Effect of Inhibitor (Retardant) on the Gel-Time and Consistency of PSX-10 in Jar Tests

% Catalyst (by weight)	% Inhibitor (by weight)	Gel-Time	Comments
1.66	0.0	6 hrs	Rigid, rubbery gel
1.66	0.25	26-29 hrs	Rubbery, slightly sticky gel
1.66	0.48	70 hrs	Very sticky, undercrosslinked gel
1.62	1.0	>16 days	Very viscous liquid
1.62	2.0	Never?	Completely ungelled

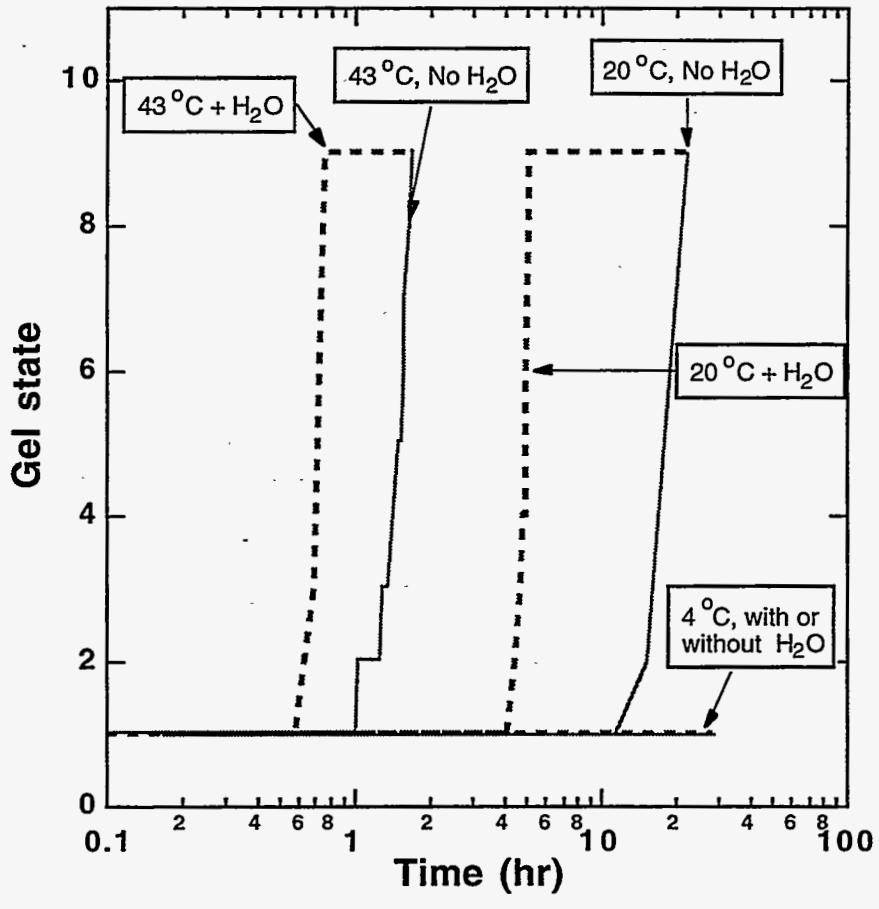

Figure 3.9. Gel time curves for PSX-10 at 4, 20 and 43 °C, with and without water, 1.25% catalyst.

4. SITE DESCRIPTION

The test site was located in central California on the property of the Los Banos Gravel Company. The subsurface geology is very similar to that at the Hanford reservation. In this section we describe the site in terms of its geological, physical and geochemical characterization. We also discuss the geochemical characteristics of the soil types, and how their variability may affect the adaptation of the design of the subsurface containment system to the site conditions.

4.1. Design Parameters, Issues, and Implications

(a) The barrier liquid injection will occur entirely in the unsaturated zone.

(b) The unsaturated zone has very low water content, which increases with depth.

(c) The site soils are extremely heterogeneous. In terms of texture, they are mainly sands and gravels (with occasional pebbles and cobbles), but also contain silt and clay lenses. The soil texture becomes finer with depth.

(d) The groundwater level at the site is very deep, i.e. about 200 ft from the surface.

(e) The average air permeability of the subsurface is 2.2×10^{-10} m^2 at the site; water permeability is 1 to 2 orders of magnitude smaller.

(f) The moisture content of the soil is very low but increases with depth from about 2.5% (by weight) to 5%, with the increase occurring at depths of 10 ft and greater. The gradation analysis showed an increase in percentage of fines from 1-2% at shallow depths to 8-9% at greater depths. An abrupt increase in fines is seen at depths greater than 10 ft.

4.2. Geological Site Characterization

4.2.1. Introduction to the Site Geology

The Los Banos quarry is located along the western flank of the San Joaquin Valley, and adjacent to the eastern margin of the central California Coast Ranges.

The quarry exploits a very large volume of volcanic, sedimentary, and metamorphic river gravels deposited within the alluvial fan of Los Banos Creek. Los Banos Creek drains a watershed containing the following Tertiary units: the Quien Sabe/Basalt Hill volcanic complex; the Franciscan assemblage; and the Great Valley Sequence of sedimentary rocks. The Los Banos alluvial fan has dimensions larger than 10×10 km^2. The fan axis is oriented NE-SW and extends through the town site of Los Banos. Surfaces within and south of the site are mantled with late Holocene Patterson gravel and terraces above the California Aqueduct (e.g. SW corner of section 31) are mantled with early Holocene and Pleistocene gravels [*Lettis*, 1982].

Prior to development of the Los Banos quarry, parts of this area were under agricultural use, planted in orchards and grasses. According to reports, the agricultural productivity of the central fan area is more than 50% lower than for more distal sites. This is thought to be the result of the very high porosity (and consequently poor water-retention) of the surfacial and near-surface deposits of the central Los Banos alluvial fan.

Geological characterization of the Los Banos quarry was undertaken to improve our understanding of the depositional environment, facies types and facies variability's of the Los Banos gravels and associated deposits and landforms. Recent aerial photography was inspected and the history of the site was discussed with the quarry operator. The field site proper and its immediate and regional surroundings were also inspected. Gravel quarry faces were inspected and described and vertical sampling profiles of the three primary shallow surface deposits were collected and carefully photographed. Archival photography was completed across the vicinity of the silica injection test area in June 1995.

4.2.2. Character of the Deposits

We have examined and sampled the deposits which are exposed along the quarry wall in the area of the grout injection test site, and in the quarry area immediately to the south of the test site. The deposits are primarily coarse sands and gravels, ranging from massive (poorly bedded) to well bedded, and appear to be essentially flat-lying and undeformed.

Figures 4.1 shows a panoramic photograph of the Los Banos quarry, and **Figures 4.2** shows a soil profile demonstrating the extreme soil heterogeneity at the injection site site. Note that in **Figure 4.1** the length of tape is 3.2 m. The scale to the left of **Figure 4.1** can be estimated from the approximately 2-m-height of the person in the figure.

Figure 4.1. Panoramic view of the area of the proposed Los Banos site of the field demonstration.

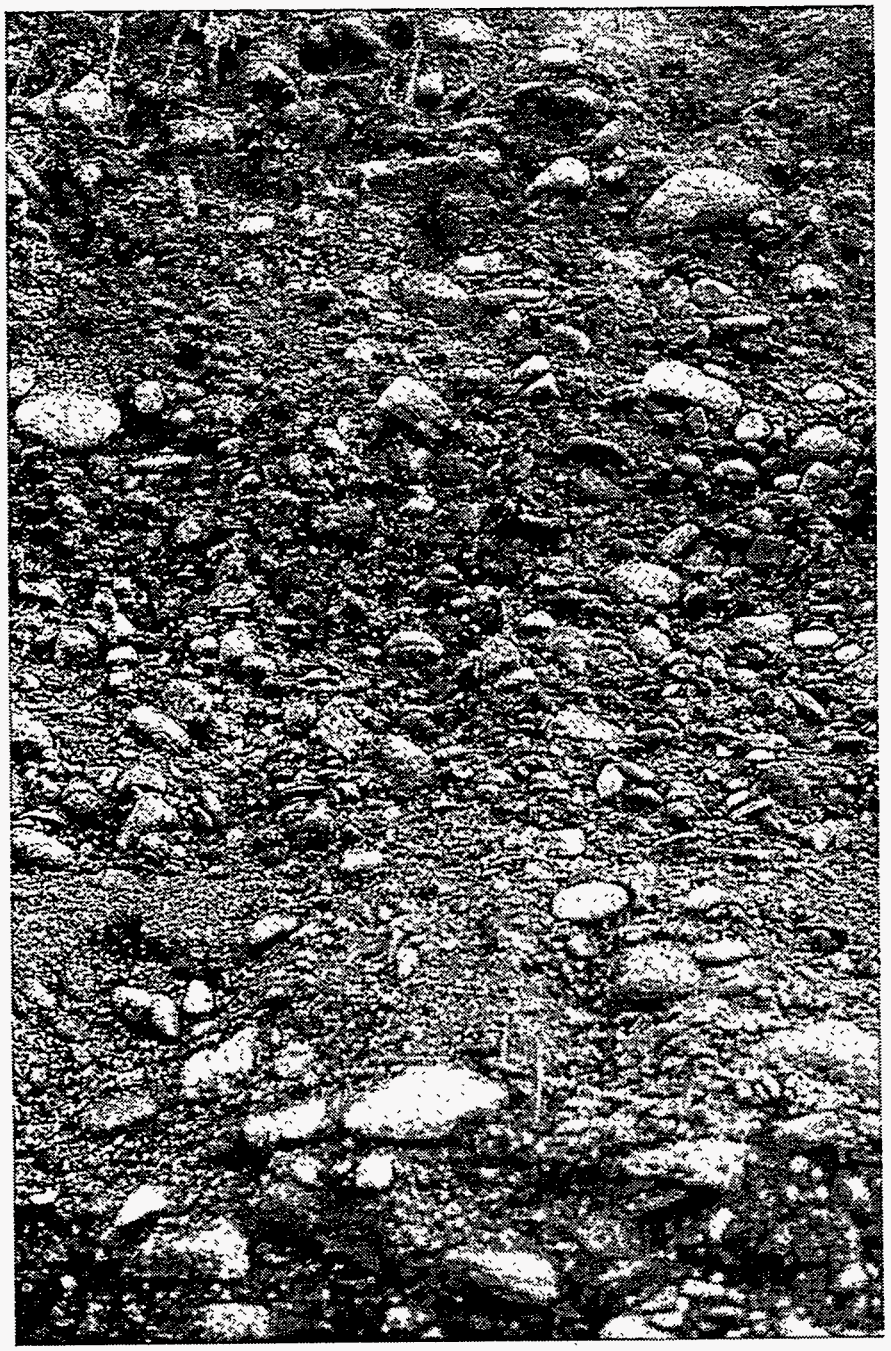

Figure 4.2. Close-up of a pit high wall at the Los Banos site showing the extreme heterogeneity of the subsurface.

We have subdivided the deposits into three units (A, B, and C) that are recognizable and continuously exposed along the quarry wall. A lower unit, unit C, consists of light-brown poorly sorted coarse sand and gravel, the base of which is covered by talus at the foot of the quarry wall. A middle unit, unit B, consists of grayer and generally better sorted gravels and sands of variable thickness ranging between ~0.3 and 2.7 m, and includes abundant coarse- and fine-grained lenses. The lower contact of Unit B with unit C is locally well-defined, sometimes marked with large cobbles, but in places is gradational and uncertain; the upper contact with unit A, where unit A is present, is generally sharp.

The upper unit, unit A, is a light-brown finer-grained deposit of poorly sorted fine to medium sand and silt, with isolated gravel or cobbles within the much finer matrix. Its thickness is uncertain, as it has been partially or entirely stripped from the surface in places, and in other places appears to have been placed by quarry activities in anomalously thick piles (**Figure 4.1**). Where the ground surface appears relatively less disturbed, the thickness of unit A is on the order of 1 m.

Large gravel and cobble clasts of the three units are commonly set in a sandy matrix. In units B and C, clast sizes are characteristically between 1 and 6 *cm*, but commonly range up to 10 cm. Rare to common larger cobbles and small boulders are present. Clasts are often tabular and aligned sub-parallel to stratification; the matrix is predominantly coarse sand (0.5-1 mm). Unit C typically has a larger component of sandy matrix than B, and poorer sorting. Gravel clasts of unit A are smaller (rarely larger than 1 -3 cm) and generally much less abundant than in the lower units (except for occasional coarse lenses); the matrix is very fine to medium sand (<0.5 mm) and silt.

Clast provenance is essentially the same in the 3 units, reflecting the major rock types outcropping in the Coast Range watershed of Los Banos Creek. These include basalt, andesite, and pink and gray rhyolitic tuff of the 7.5-10 million-year old Quien Sabe Volcanics (some of which was probably derived from the Basalt Hill outlier of the Quien Sabe volcanics located to the south of San Luis Reservoir); sandstone from the Great Valley Sequence; and less abundantly graywacke sandstone, schist, red chert, and possibly greenstone from the Franciscan assemblage.

The finer, sandy fraction of the deposits comprises varicolored lithic fragments of these rock types, along with grains of feldspar, quartz, and quartzite derived from them. Shapes of the larger clasts often correlate with rock type, with clasts composed of sandstone or schist commonly elongate or tabular reflecting internal sedimentary structure, and volcanic clasts commonly round. In the coarse clast fraction of unit C, round volcanic clasts dominate, and are apparently more abundant than in the upper units.

All three units, and B and C in particular, are internally heterogeneous, with discontinuous and lenticular coarser and finer strata, and occasional clast imbrication structures and lenses of well-sorted cross-bedded sands. These features, along with locally channeled and irregular contacts between strata and lenses, indicate deposition from or reworking by flowing water. The deposits range in degree of cohesion from completely unconsolidated (much of B) to somewhat indurated (C and A).

Induration, where present, is caused by infiltration (illuviation) of clay into pores between sand grains; a fine film of yellow-brown clay can be seen binding the sandy matrix in most samples, and the film becomes a thicker and more continuous coating in direct relation to the degree of induration. The clay coating must affect porosity and, in more indurated samples, permeability; however, in most cases, the clay does not appear to fill pores completely, and possibly does not reduce the permeability of these deposits markedly.

4.2.3. Depositional Facies and Stratigraphic Correlation

The sands and gravels exposed at the quarry are fluviatile alluvial fan sediments deposited near the western edge of the Coast Range alluvial plain, on a distributary lobe of Los Banos Creek adjacent to its present channel. Based on the detrital composition and sedimentary structures described above, they correspond to the middle to upper fan facies of *Lettis* [1982]. Most are stream channel deposits, possibly also including sheetflow deposits where relatively fine-grained planar beds are present. However, the finer-grained sediments of unit A (and locally in unit C), characterized by poor sorting, poor stratification, and matrix-supported cobbles, are probably mudflow deposits, also consistent with middle to upper fan facies.

Stratigraphically, the deposits belong to the late Holocene Patterson alluvium, which ranges in age from several thousand years to the present century. Bordering terraces are of late Pleistocene to early Holocene San Luis Ranch alluvium, which is very similar to the Patterson alluvium in composition and range of sedimentary characteristics [*Lettis*, 1982].

4.3. Chemical Site Characterization

In developing permeation grouting technology, it is important to characterize the geologic media to be injected for the purpose of designing and interpreting laboratory studies, planning field tests, and establishing test protocols for general implementation of the technology. The chemical characterization tests may include:

- Exchangeable Cations
- Cation Exchange Capacity
- pH Measurements On Saturated Soil and 1:1 Soil/Water Mixture
- Soil Saturation Extract (or Soluble Salts)
- Hydroxylamine HCl Extractable Hydrated Ferric Oxide (HFO)
- Calcite and Gypsum Content
- Organic Content
- Mineralogy (by Optical Microscopy and X-Ray Diffraction)

The information obtained can be used to model the response of the geologic medium when subjected to incursion by various wastes and to predict the long-term interactions between the grout, waste and the soil minerals. Unconsolidated surficial geologic deposits overlying bedrock are

commonly quite heterogeneous. The heterogeneities can vary in scale and frequency depending on the nature of the deposit. Furthermore, deposits undergo further modification subsequent to emplacement through the growth of overlying soil zones, the nature of which are strongly related to the prevailing climate. Hence, it is desirable to sample both laterally and vertically to ensure that heterogeneity is adequately characterized.

Chemical characterization studies were conducted on -10 mesh screened samples from the sand and gravel quarry of the test site [*Moridis et al.*, 1995a]. Grab samples taken form the quarry faces were used. For budgetary reasons, no attempt was made during this initial step to collect representative samples throughout the full height of the quarry faces. Nor were all of the measurements described above completed initially. The analyzed exchangeable cations, cation exchange capacity, and saturation extracts are given below in **Tables 4.1** and **4.2**.

A preliminary inspection of the data in **Tables 4.1** and **4.2** indicates that the Los Banos soils contains elevated concentrations of magnesium and ammonium exchangeable cations. The former is probably due to the provenance of the gravel, which is derived from a mafic Tertiary igneous complex and Franciscan serpentinites in the Coast Range immediately west of the site, and which are exposed in the catchment basin of Los Banos Creek. The gravel deposits form part of a Quaternary outwash fan created by the creek . The latter is consistent with the relatively high concentration of ammonium, sulfate and nitrate in the soil saturation extract, and suggests contamination by fertilizers applied to the cultivated land previously overlying the present site of the gravel quarry.

Table 4.1. Cations and Cation Exchange Capacity of the Los Banos Soil

Cation	Units	Measurement
Sodium	ppm	34
Potassium	ppm	110
Magnesium	ppm	380
Calcium	ppm	1700
Strontium	ppm	14
Ammoniacal Nitrogen	ppm	94
Aluminum	ppm	6.6
Cation Exchange Capacity	meq/100g	7.7

Table 4.2. Saturation Extracts of the Los Banos Soil		
Analysis	**Units**	**Measurement**
pH		8.0
Electrical Conductivity	mmho/cm	1.5
Bicarbonate Alkalinity	ppm	160
Carbonate Alkalinity	ppm	<1
Hydroxide Alkalinity	ppm	<1
Calcium	ppm	54
Magnesium	ppm	18
Sodium	ppm	260
Potassium	ppm	5.6
Strontium	ppm	0.2
Ammonical Nitrogen	ppm	23
Sulfate	ppm	230
Chloride	ppm	240
Nitrate	ppm	64
Phosphate	ppm	<5
Silica	ppm	48

4.4. Physical Site Characterization

Information on the physical properties of soils at the Los Banos site had been obtained during the first small-scale field demonstration [*Moridis et al.*, 1995*a*]. These analyses had provided important information and were not repeated in this effort because the available information was deemed sufficient. The physical characterization includes information on moisture content, particle size distribution and permeability.

4.4.1. Physical Properties of Soils at the Test Site

After bulb excavation in the first small-scale field demonstration [*Moridis et al.*, 1995*a*], grab-bag samples of ungrouted soil had been taken at various depths from locations adjacent to the grouted soil bulbs. Both moisture content and material gradation analyses had been performed on these samples. It must be pointed out that the larger cobbles had been removed from the grab bags, and thus are not represented in the results.

Results are shown in **Figure 4.3** and **Table 4.3** respectively. The moisture content of the ungrouted soil appears to be very low but increases with depth from about 2.5% (by weight) to 5%, with the increase occurring at depths of 10 ft. and greater. The gradation analysis showed an increase in percentage of fines from 1-2% at shallow depths to 8-9% at greater depths. An abrupt increase in fines is seen at depths greater than 10 ft. An increase in moisture content with increasing percentage fines would be expected. The gradation analyses confirmed both the injectivity profile and visual field observations (that the amount of fines increased with depth) made at the time of the first small-scale field demonstration [*Moridis et al.*, 1995a]. A corresponding decrease in permeability would also be expected in association with the increased amount of fines.

4.4.2. Permeability Distribution

One of the most important design parameters (if not the most important) is permeability and its distribution. Pre-injection characterization of bulk soil permeability is necessary for the selection of the appropriate grout composition and determination of optimum spacing. If soils are highly permeable it is desirable for the grout to gel more quickly so that it remains in the desired region. If permeability is low, it is desirable to have the grout gel less quickly so that it can enter the intended region before gelling. Permeability, coupled with its distribution, dictate the well spacing for optimum coverage.

In the first field test *in-situ* measurements had been made [*Moridis et al.*, 1995*a*] to characterize air permeability of the soil in the grout injection region prior to the injection. These measurements were used as the basis for this study because the available information was judged sufficient. In regions of relatively low soil moisture content, soil air permeability may be used as a proxy for total permeability, especially in cases where permeability is governed by flow through fast paths.

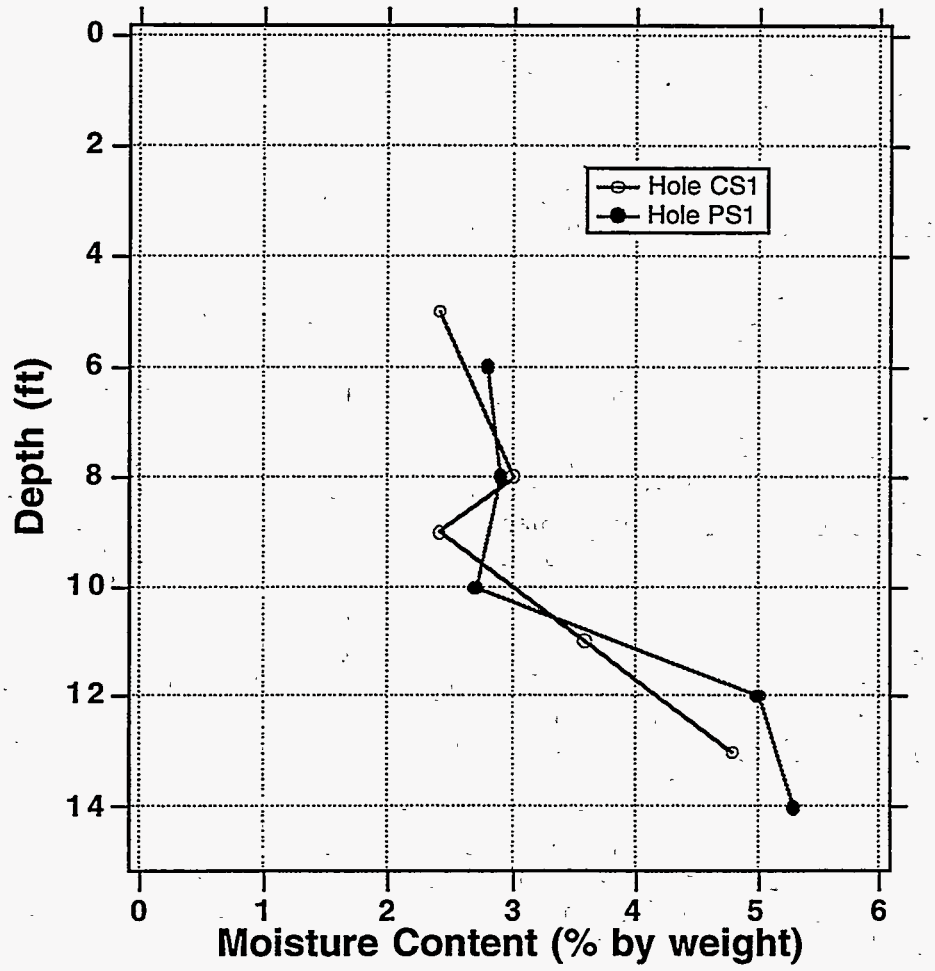

Figure 4.3. Variation of moisture content with depth at the Los Banos site.

Measurements were made using two different techniques: the standard single-well steady-pressure permeameter (SSP) test and a dual-well dynamic pressure (DDP) technique recently developed at LBNL [*Garbesi*, 1994]. The SSP technique introduces air into a well at a constant rate, using Darcy's law and the assumption of a semi-infinite homogeneous medium to estimate permeability from the measured disturbance pressure and air flow rate. The DDP technique uses the propagation time for a sinusoidally oscillating pressure signal to travel from a source well to a detector well as a measure of the air permeability.

Both SSP and DDP measurements sample over a finite region of the soil. A discussion of how these different techniques *sample* permeability from a homogeneous soil illustrates a number of important advantages of using the DDP technique for a pre-injection site diagnostic. It also illustrates why single-well steady-pressure measurements can yield seriously misleading results.

Table 4.3. Summary of Gradation of the Los Banos Site Soils			
Sample ID	Percentage by Dry Weight		
	Gravel	Sand	Silt
PS1-NW-6	16	82	2
PS1-NW-8	39	59	2
PS1-SW-10	54	45	1
PS1-SW-12	49	43	8
CS1-S-14	46	48	6
CS1-S-5	46	52	2
CS1-W-8	33	66	1
CS1-W-9	47	52	1
CS1-NW-11	42	55	3
CS1-E-15	51	42	4
LB-D	17	74	9

The sampling scale of the SSP technique is determined by the pressure gradient induced in the soil surrounding the well. For a point pressure source in a homogenous medium, the pressure diminishes with inverse distance from the source ($P \propto 1/r$). The approximately spherical SSP flow geometry results in a large pressure gradient adjacent to the well that diminishes rapidly with distance. Since the flow is proportional to the pressure gradient, the SSP technique primarily yields information about soil permeability in the immediate vicinity of the well. This fact makes the technique vulnerable to soil disturbance during well installation and to local small-scale heterogeneities. A greater limitation is imposed by the effective size of the sampling region, which depends upon the size and geometry of the well tip. For the wells used in this experiment, the sampling radius is 1 *m*—as determined by the distance at which the disturbance pressure field has fallen to 0.5% of its value at the probe tip. This choice has shown good agreement between SSP measurements and DDP measurements made in the same soil over the same scale.

The primary advantage of using DDP measurements as a pre-injection diagnostic for soil permeability is that it can gather information about permeability at a user-selected scale. The sampling scale of DDP measurements is the separation distance between the source and the detector wells. At the Los Banos site, successful measurements were made at all sampling scales attempted (up to 6.5 m).

Previous field studies have shown that soil air-permeability can depend on sampling scale [*Garbesi*, 1994]. In particular, if measurements are made at a small scale and averaged, the estimated permeability can be considerably smaller than if measurements are made at larger scales and averaged. These results are interpreted as resulting from the fact that if flow occurs over larger scales, the flow is more likely to intercept spatially dispersed fast flow paths, than would be the case at smaller scales— thus allowing larger flow rates.

In the grout injection experiment, the liquid grout has access to potential fast flow paths in the entire injection area (a scale of many meters, that we refer to here as the system scale). It is therefore sensible to characterize soil air-permeability at the system scale as a *pre-injection diagnostic*. In practice, DDP measurements are made over a range of scales and spatial orientations to (a) determine if permeability is significantly scale-dependent over the likely range of scales ultimately to be occupied by the grout, and (b) to check for possible anisotropy in permeability that could significantly determine the ultimate geometry of the grouted soil. For example, significantly larger horizontal than vertical permeability could result in the grout gelling in a thin lens.

Another advantage of the DDP technique stems from the fact that the characterization of the effective soil permeability over the path between the wells gives relatively equal weighting to all locations along the path, rather than being heavily weighted by soil conditions adjacent to the source well as in SSP measurements. The reason for this is that, in a homogeneous medium, the signal propagation velocity used to determine permeability is relatively constant, independent of distance from the source. In a heterogeneous medium, the signal is slower in low permeability regions and faster in high permeability regions. Therefore, the integrated measure of permeability resulting from the signal travel time between the two wells gives a rational measure of the effective permeability of the path.

In summary, the DDP technique offers the following advantages over SSP measurements:

- Permeability can be sampled at the system scale (many meters) using DDP measurements, giving an indication of the permeability *seen* by the injected barrier liquid. SSP measurements tend to sample on significantly smaller scales.
- Permeability may be sampled on paths having arbitrary orientation in the soil, allowing the easy exploration of soil anisotropy.
- The DDP measurement system gives relatively equal weight to all points along the path between the two wells. This makes the DDP system much less vulnerable to measurement uncertainties introduced by disturbance of the soil near the wells or to localized heterogeneities.

- With the same number of probes, the DDP method obtains considerably more information about the soil, including exploration of anisotropy, scale effects and many different possible combinations of paths. Given N probes, the number of non-redundant pairs for DDP paths is $(N^2 - N)/2$, whereas, only N SSP measurements are unique. For example, 8 probes can imply 28 unique DDP paths.
- The possibility of localized heterogeneity of permeability that has little effect on the bulk movement of contaminants through the soil, can be explored directly by making DDP measurements that cross the region of interest.

Table 4.4 indicates all of the source-to-detector paths (six wells, shown by well ID) used for DDP measurements and the results of permeability measurements made along those paths [*Moridis et al.*, 1995a]. Repeated measurements indicated a worst-case uncertainty characterized a mean value times or divided by 2.5. In cases where repeated measurements were made over a given path, the arithmetic mean of repeated measurements is indicated in the table.

To examine the possibility of anisotropy in soil permeability, **Figure 4.4** shows permeability data presented for paths with different zenith angles (ζ) and having path lengths between 2.4 and 3.5 m. The zenith angle is defined as the angle between a ray that points directly upward from a source probe and a ray that points from the source probe to the detector probe. Measurements with $\zeta = 90^\circ$ are therefore made on a horizontal path. Measurements at ζ greater than or less than 90° capture some component of vertical permeability. The data presented in **Figure 4.4** show no obvious trend with ζ, therefore anisotropy is not considered to be significant at this site.

The results of all of the DDP measurements at all measurement scales are presented graphically in **Figure 4.5.** On first inspection, one might conclude that there is some scale dependence of permeability over the range of scales inspected by DDP sampling (1.0 – 6.5 m), because of the cluster of low permeability data appearing in the lower left of the plot. On closer inspection, however, we find that all of those data are for DDP measurements made using a single well (CS1) as either a source or detector. The cause of this low permeability cluster could be that the CS1 well was not effectively cleared after installation, or that the CS1 well terminated in a low permeability zone of the subsurface.

Another advantage of the DDP technique is that measurements can be nested within one another. Normally the results of all independent measurements are included in a calculation of some average measure of the bulk permeability of the soil. The averaging system depends upon the configuration of the soil. For heterogeneous systems with lognormally distributed permeabilities k_i, stochastic models which allow only small perturbations on uniform flow yield a measure of macroscopic permeability determined by $m_G(1+\sigma^2/6)$, where m_G is the geometric mean and σ is the standard deviation of the $\ln(k_i)$. Depending upon the assumptions of the stochastic distribution and the nature of flow, mean flows are found to lie somewhere between the geometric and arithmetic means [*Dagan*, 1989].

Table 4.4. Permeability Measurements Using the Dual-Well Dynamic Pressure (DDP) Technique

DDP Path	Permeability (m^2)
AP1 - CS1	6.3×10^{-12}
AP1 - CS2	3.5×10^{-10}
AP1 - AP3	1.6×10^{-10}
AP1 - PS1	1.1×10^{-10}
AP1 - PS2	1.1×10^{-10}
AP2 - AP1	1.8×10^{-10}
AP2 - AP3	1.2×10^{-10}
AP2 - AP4	2.3×10^{-10}
AP2 - PS1	1.1×10^{-10}
AP2 - PS2	1.2×10^{-10}
AP3 - AP4	1.7×10^{-10}
AP3 - CS1	6.8×10^{-12}
AP3 - CS2	3.9×10^{-10}
AP3 - PS1	3.3×10^{-10}
AP3 - PS2	3.2×10^{-10}
CS1 - AP2	7.9×10^{-12}
CS1 - AP4	9.9×10^{-12}
CS1 - CS2	1.7×10^{-12}
CS2 - AP2	2.5×10^{-10}
CS2 - AP4	4.3×10^{-10}

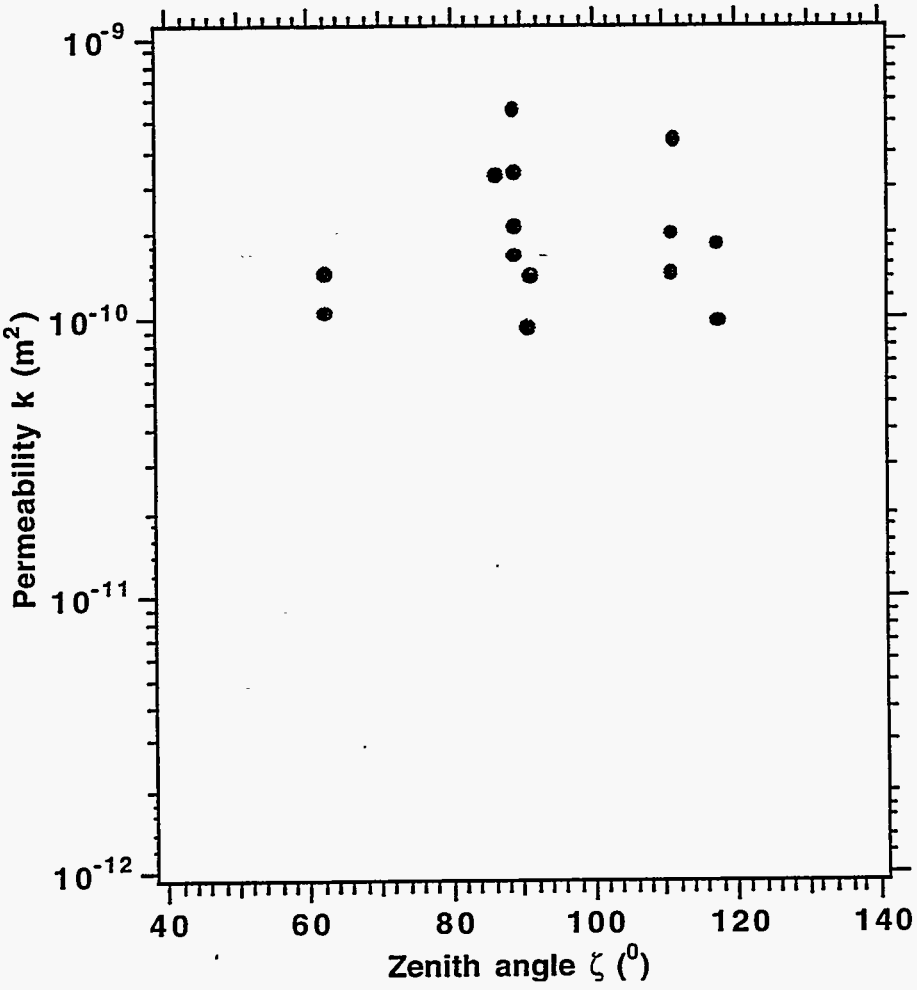

Figure 4.4. Permeability relationship to the zenith angle ζ for path lengths between 2.4 and 3.5 m.

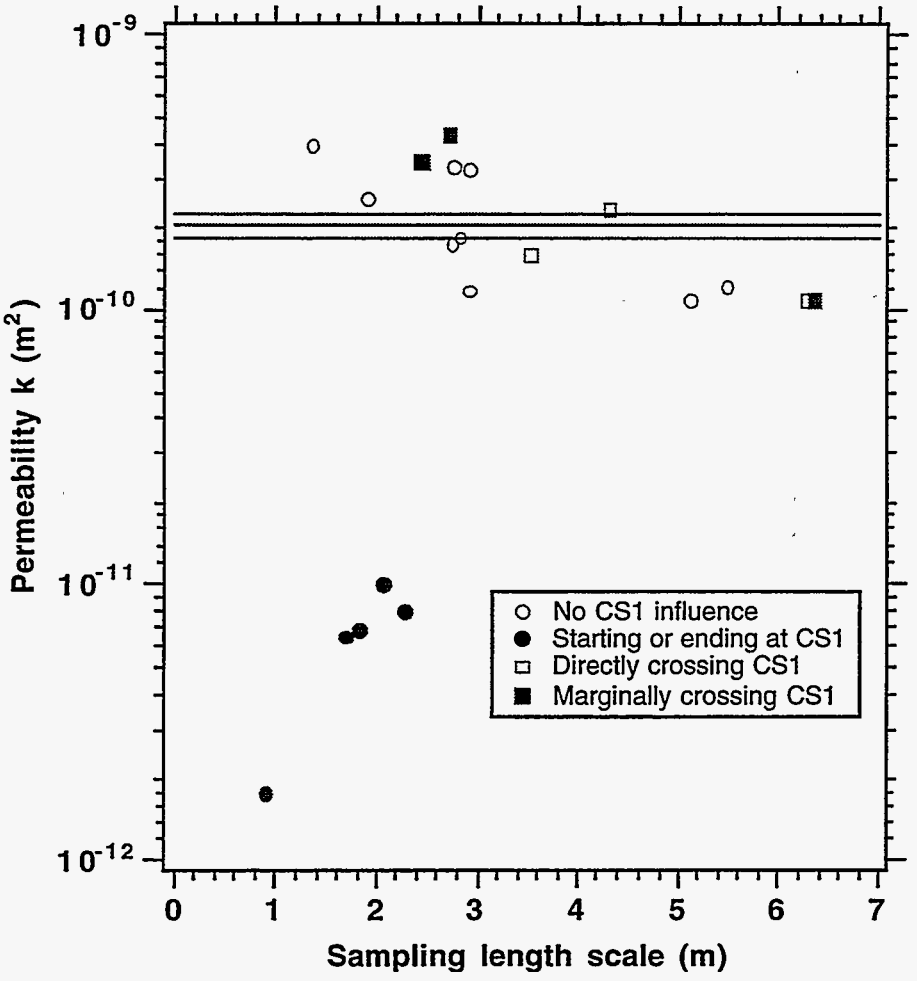

Figure 4.5. Permeability relationship to the zenith angle ζ at all measured scales.

The model assumes the k_i are uniquely defined for different points in space. This approach is not appropriate for interpreting mean results of the DDP measurements since the measurement regions overlap and in some cases are nested. Inspection of the well array, however, indicates that measurements on paths that cross directly over or near CS1 do *not* indicate similar low permeabilities (**Figure 4.5**). Indeed there is *no* indication of any reduction in permeability for paths crossing this region.

Our interpretation is therefore that the perturbation at CS1 has little relevance on the larger scale of the experiment (no matter what the cause). That is, fluid that flows on a scale of many meters would simply move around the low permeability region, with little net effect. Therefore, it makes more sense to ignore these data on the experiment scale, than to include them in some measure of the mean permeability. Ignoring the CS1 data, the arithmetic mean m_A permeability and the geometric mean m_G permeability are the same to within sampling error, yielding an average permeability for the region-to-be-injected of 2.0×10^{-10} m^2.

The results of the standard steady-pressure (SSP) measurements are presented in **Table 4.5**. Summary statistics of all SSP and DDP measurements (including and excluding CS1) are presented in **Table 4.6**. From these statistics (especially the relative sizes of the geometric standard deviations σ_G) we note that the DDP data set without the CS1 contribution provides a more representative measure of the subsurface permeability than the entire DDP data set or the SSP data set. Finally, we note that the average SSP estimate of permeability is lower than the DDP estimates. This is probably due to the fact that the SSP measurements are made at smaller scales than most of the DDP measurements. In our experience from previous measurements in natural soils, the sensed/measured permeability can decrease rapidly at distances shorter than 2 m from the injection point. Previous studies have shown good agreement between SSP and DDP measurements made at the same scale [*Garbesi*, 1994].

In **Figure 4.5** the central line represents the best estimate of the soil air-permeability at the scale of the injection experiment (the m_G of non-CS1 data, i.e., excluding the open diamonds). The upper and lower lines represent the m_G of the non-CS1 multiplied or divided by (respectively) the uncertainty in the estimation of m_G (**Table 4.6**). Note that the worst-case uncertainty in the individual measurements, as determined from repeatability experiments, is quantified by a factor of 2.5 by which to multiply or divide the measured k values.

It must be pointed out that the DDP air permeability measurements discussed here reflect the permeability of the most permeable pathway between source and receptor and should not be assumed to coincide with the water permeability values. Water permeability measurements are usually significantly lower (1 to 2 orders of magnitude on average) than the air permeability values.

Table 4.5. Permeability Measurements Using the Single-Well Static Pressure (SSP) Technique

Well Name	Permeability (m^2)
CS1	4.4×10^{-13}
CS2	1.3×10^{-10}
PS1	9.1×10^{-11}
PS2	6.9×10^{-11}
AP1	7.7×10^{-11}
AP2	9.1×10^{-11}
AP3	9.9×10^{-11}
AP4	8.0×10^{-11}

Table 4.6. Summary Statistics of SSP and DDP Permeability Measurements at the Los Banos Site

Statistic	Technique and Data		
	SSP - all	DDP - all	DDP - no CS1
m_A	7.9×10^{-11}	1.7×10^{-10}	2.2×10^{-10}
m_G	4.6×10^{-11}	7.6×10^{-11}	2.0×10^{-10}
σ_G	6.6	7.6	1.7
Uncertainty - $\sigma_G^{1/\sqrt{N}}$	1.9	1.6	1.1

4.5. Evaluation of Chemical, Physical and Mineralogical Data of the Geologic Media

The geochemical, mineralogical and physical data, collected at a given site, permit evaluation of the chemical characteristics of the geologic medium. Such information is valuable in predicting the behavior of the geologic medium in response to the injection of grouts, and must be performed before reactive chemical and physical transport models can be used either to predict the behavior of grouts during injection, or to investigate other transient chemical phenomena a given site.

Earlier evaluations of soil profiles [*Narasimhan et al.*, 1992] have demonstrated that a modification of the MINTEQ code is particularly suitable for the characterization of the chemical properties of unconsolidated surficial geologic media. The latest version of MINTEQ incorporates a clay polymer model developed by *Sposito* [1986], *Mattigod and Sposito* [1978], and *Krupka et al.* [1988] to describe ion exchange phenomena, and a simplified surface complexation model to describe the adsorption of ionic and molecular species on iron oxides, described by *Krupka et al.* [1988].

The approach to be taken in modeling the geochemistry of the quarry sand samples consists of the following steps:

(1) Evaluation and conditioning of the saturation extract chemical analyses,
(2) Incorporation of thermodynamic constraints, e.g. CO_2 partial pressure and saturation with respect to minerals such as calcite, gypsum or halloysite.
(3) Reconstitution of the original pore water composition in the unsaturated zone.
(4) Distribution of species and calculation of thermodynamic parameters, e.g. the saturation indices of known primary and secondary minerals, and potential secondary minerals.
(5) Calculation of the distribution of species on the ion exchange sites in clays and comparison of total ion exchange and adsorption sites (on HFO) with measured extractable bases.

Each step is described in greater detail in the following subsections.

4.5.1. Interpretation of the Saturation Extract

The procedure adopted in evaluating the saturation extract is summarized in the form of a flow chart in **Figure 4.6**. Details of the procedure follow.

Partial chemical analyses of the saturation extracts are given in **Table 4.2**. Analysis for $B(OH)_3(aq)$, Al^{3+} and Fe^{3+} were not performed. Although these species are important in evaluating equilibrium with soil matrix minerals, they are usually present in saturation extracts only at very low concentrations and contribute negligibly to electrical charge balance calculations. Furthermore, the resulting analyses for these species are difficult to interpret. Hence, they were not measured in this characterization. In order to augment the chemical analysis, additional assumptions regarding saturation with respect to certain minerals must be made.

The partial pressure of carbon dioxide in the saturation extract can be calculated from the bicarbonate alkalinity and pH. Because the carbon dioxide contribution from bacterially oxidizing organic matter can be significant in the subsurface,. the partial pressure of carbon dioxide could easily be as high as 10^{-2} atmosphere. However, in regions with low rainfall, the organic content of coarse river gravels or outwash fans, as at Los Banos, is often quite low, of the order of 0.1 wt. percent. It would not be surprising, however, if the CO_2 partial pressure were to be less than 10^{-2} atmosphere and could even be in equilibrium with that in the atmosphere, i.e. $10^{-3.48}$ atmosphere.

Halloysite ($Al_2Si_2O_5(OH)_4$) is assumed to be present throughout the soil profile as a kaolinite precursor resulting from the weathering of potash feldspar ($KAlSi_3O_8$). Halloysite, coexisting with α-cristobalite, fixes the aluminum activity in solution. Finally, it is assumed that the ferric ion activity is determined by saturation with respect to hydrated ferric oxide, $Fe(OH)_3$, on the basis of the sand coloration. Although there is no assurance that the saturation extract equilibrated with respect to authigenic soil minerals in the short two hour equilibration period, it is assumed, as a point of departure, that such is the case.

Several checks can be made to test the validity of the saturation extract chemical analysis. The most important of these include a check on the ionic charge balance and reconciliation between calculated and measured electrical conductivity. A check on the charge balance can be readily accomplished during the distribution of species using MINTEQ. Other minor checks for consistency and reasonableness of the analysis can also be made when distributing the aqueous species, as will be discussed further, below.

The electrical conductivity of the saturation extract solutions is given in **Table 4.2.** In principle, it should be possible to calculate the electrical conductivity of a solution from a knowledge of the concentrations of the principal constituents in solution. *APHA* [1985] suggests a relatively simple method of calculating the conductivity of the solution, provided that the solution is, or has been made sufficiently dilute that the conductivity lies between 0.090 and 0.120 $mmhos.cm^{-1}$. The saturation extract conductivities range between 0.4 and 1.5 $mmhos.cm^{-1}$ which is between 3 and 12 times higher than the range of applicability. Therefore some deviation is to be expected between predicted and measured electrical conductivity. More elaborate algorithms for predicting electrical conductivity of electrolytes at higher ionic strengths are being investigated.

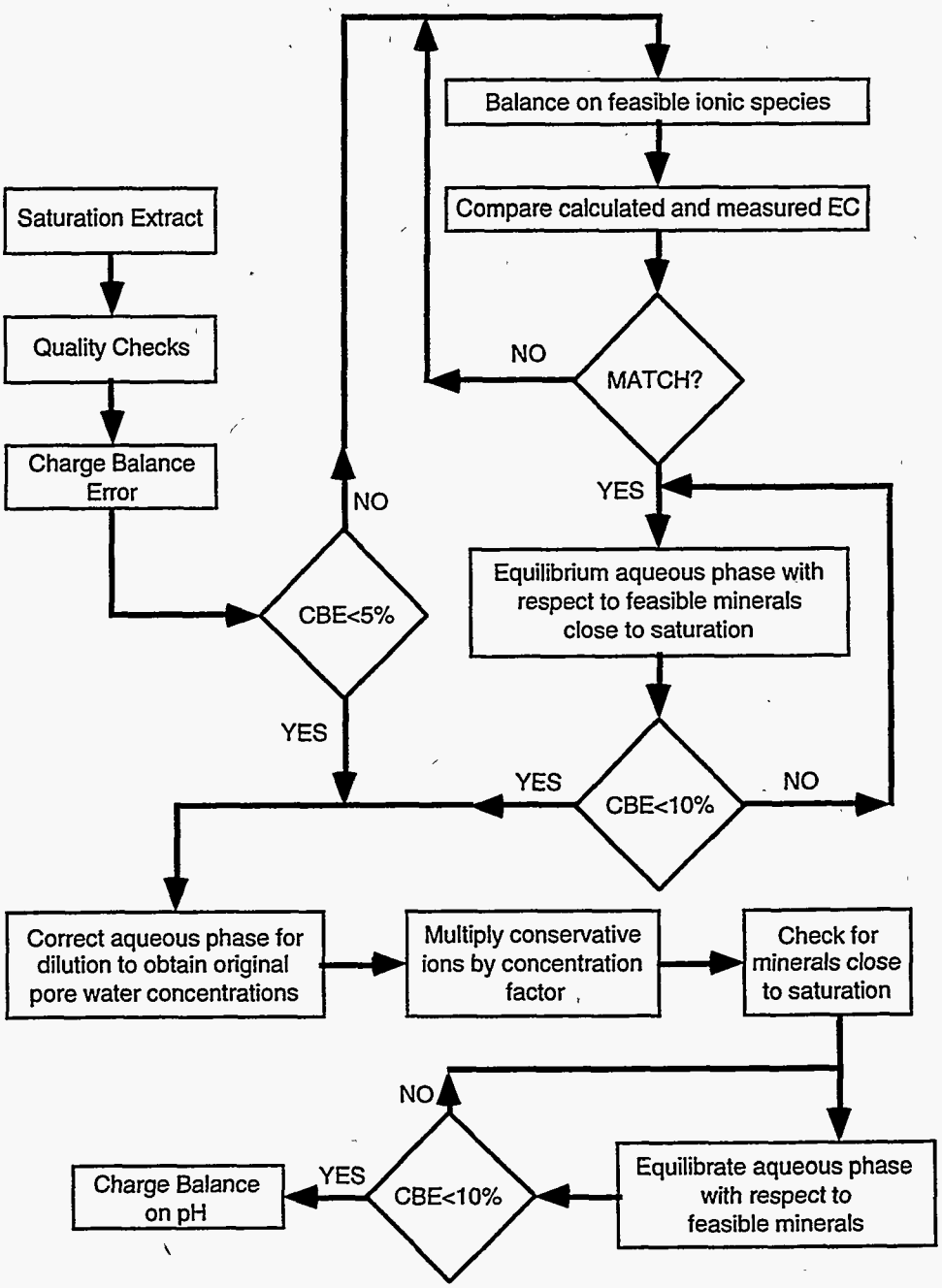

Figure 4.6. Flow chart to illustrate the procedure in evaluating soil saturation extracts.

4.5.2. Reconstitution of the Sand Pore Fluid

The pore fluid composition can be estimated by assuming that the original soil moisture is diluted to fill the porosity of the sand, The soil saturation extract composition therefore reflects this dilution, but is possibly modified through dissolution and saturation by readily soluble salts such as calcite and gypsum, and clay minerals with a large specific surface area. If, either the saturation extract is saturated with respect to any commonly occurring salts, or achieves Supersaturation during reconstitution of the original pore water composition, then it may be reasonably assumed that the original pore water was also saturated. In the case of carbonates, it is possible to test for their presence using concentrated HCl and observing the resultant effervescence, as is observed in the case of the Hanford site sand samples. The presence of other soluble salts, such as gypsum are not be so readily detected, particularly if finely disseminated and in trace amounts.

The composition of the reconstituted pore fluid is therefore computed by correcting the conservative aqueous species for the dilution to the saturation extract concentration, using the appropriate dilution factors. The minerals, calcite, α-cristobalite, halloysite, and $Fe(OH)_3$ are assumed to be saturated throughout the profile. A distribution of species will be made for each sand using the MINTEQ code, ensuring electrical neutrality by adjusting the pH.

4.5.3. Degree of Saturation of the Pore Fluid

Pore fluid saturation indices can be calculated using MINTEQ for several potential secondary minerals that occur in soil profiles in arid regions. The corresponding thermodynamic data are known to possess uncertainties of about ± 4 kJ in the Gibbs Free Energy of formation, $\Delta G^{\circ}_{f,298}$. The closeness of the saturation indices of observed minerals to zero would support the validity of the mineral thermodynamic data and interpretation of field observations. Checking for mineral saturation is a valuable secondary test for the validity of the calculated pore fluid composition.

4.5.4. Distribution of Ionic Species

As noted previously, the MINTEQ code incorporates the clay polymer model refined by *Mattigod and Sposito* [1978] and *Sposito* [1986]. The model was applied by *Krupka et al.* [1988] to permit calculation of the distribution of species on the exchangeable sites of clays, using the Vanselow convention to calculate the activity coefficients of the species occupying the cation exchange sites [*Vanselow*, 1932; *Sposito*, 1986]. MINTEQ treats the ion exchange sites as pseudo-aqueous species for the distribution of species between the exchange sites and the aqueous phase. Therefore, the concentration of exchange sites is defined in relation to the mass of aqueous phase present in the soil. Hence the extent of water saturation of the soil, the porosity, and the concentration of exchange sites, i.e. the cation exchange capacity of the soil, must be known.

Ion exchange constants, relating the activity of given cations on the exchange sites with their activities in solution have been compiled [*Morrey*, 1988] and are incorporated as part of the thermodynamic data base used by MINTEQ. It is therefore possible to calculate the distribution of cation exchange sites for each sand sample. The total concentration of HFO-adsorption sites in the samples can be estimated from the hydroxylamine HCl determination of soluble ferric iron in the sample, or with somewhat greater uncertainty from data compiled by *Gile and Grossman* [1979]. In common with the ion exchange sites, MINTEQ treats the HFO-sites as pseudo aqueous species. A corresponding thermodynamic data-base incorporating adsorption constants for various cationic and anionic species is also included with the MINTEQ code. MINTEQ may therefore be used to compute the distribution of ionic species on both the exchange and the HFO-sites in each soil horizon.

The extractable bases, obtained by leaching a soil sample with 1N ammonium acetate, have been measured for each sand sample and are reported in **Tables 4.1** and **4.2**. The bases represent the sum of all species leached from the soil by ionic exchange of ammonium ion on clay cation exchange sites and surface adsorption sites, as well as enhanced dissolution of calcite, and possibly other Mg and Ca containing phases due to acetate complexing of calcium and magnesium. The total concentration of extractable bases is therefore likely to be much greater than the cation exchange capacity determined from total sodium ion exchange and adsorption.

In order to correct for this effect, it is assumed that the excess in concentration of the extractable cations over the cation exchange capacity is due to the dissolution of calcite. Hence, the concentration of exchangeable Ca^{2+} is obtained by subtracting the difference between the total extractable cations and the cation exchange capacity from the total concentration of extractable Ca^{2+}.

4.6. Application of Evaluated Data to Permeation Grouting

Upon completion of the procedures outlined above, laboratory column tests can be designed to validate the findings through comparison with one dimensional reactive transport computer simulations. These tests can replicate conditioning, e.g. pre-flush procedures for the geologic medium, which are required when using certain colloidal silica formulations, or they can be used to predict how certain colloidal silica formulations are likely to respond, in terms of gelation time at a given site. Satisfactory validation of laboratory tests will then permit the simulator to be used to explore injection strategies at other sites with different physical and chemical characteristics of the geologic medium.

In previous subsections, the results of laboratory and *in-situ* tests with sand samples from Los Banos were presented. The evaluated data can also be used in simulations to predict interactions between liquid waste or the emplaced grout and the geologic media.

The one dimensional reactive transport simulations can be conducted using either a proprietary simulator, FASTCHEM™, developed at Pacific Northwest Laboratories for the Electric Power Research Institute, [*Kitanidis et al.*, 1991; *Narasimhan et al.*, 1992], or HYDROGEOCHEM [*Yeh and Tripathi*, 1990; 1991], which is presently being revised and improved at Sandia National Laboratories, Albuquerque, New Mexico. Interactions between the waste or emplaced grout and the geologic medium are preferably conducted, at least initially, using reaction progress simulators, such as EQ3/6 [*Wolery*, 1992: *Wolery and Daveler*, 1992] or CHILLER [*Reed and Spycher*, 1989]. This numerical simulation work is currently in progress.

5. DESIGN SIMULATIONS

In this section we investigate numerically the emplacement and performance of a barrier system underneath a leaking tank. The scenarios we investigated were consistent with a leaking underground storage tank at the Hanford reservation (the initial target of the subsurface containment technology) in a deep unsaturated formation dominated by sands and gravels.

Several sets of simulation runs were conducted, and the effects of varying a number of design and operational parameters were investigated. In this section, however, we present simulation runs obtained when using the optimum set of design parameters which meet field feasibility criteria.

The LBNL containment technology has to be adapted to the specific needs at a given site. Each contaminant problem requires a different remediation strategy. The primary purpose of the subsurface barrier may be, for example, to control the groundwater pattern, to prevent the spread of an existing plume, to facilitate cleanup operation, to immobilize the contaminant, or to provide a long-term in-situ containment.

At Hanford, the leakage of hazardous, radioactive wastes from underground storage facilities requires a containment technology that

- is effective in preventing downward migration of contaminants,
- may facilitate subsequent cleanup operations and/or permanent in-situ containment,
- is environmentally benign and itself resistant to chemical and radiological attack,
- can be emplaced without mobilizing the contaminants and without affecting the structural integrity of the tanks.

Finally, the implementation of the containment technology has to be technically feasible and economically acceptable.

5.1. Barrier Fluids and Emplacement Method

The high ion concentrations in the Hanford soil does not cause premature gelation of either the Colloidal Silica (CS) grout (DP5110) or the PolySiloXane (PSX-10) to be used in this field demonstration. This is due to the special formulation of these products which through surface modification (CS) or catalyst selection (PSX) alleviate potentially adverse geochemical effects. In terms of numerical simulation, both CS and PSX are treated very similarly because they have very similar properties. Therefore, although our simulations were based on a CS system (as the most likely barrier liquid due to its considerably lower cost), the results are applicable to PSX systems.

The barrier fluid emplacement technologies which have been considered are permeation grouting from arrays of vertical, inclined, and horizontal wells, controlled delivery hydrofracturing, and jet placement systems. For conditions similar to those in Los Banos (and at Hanford), permeation grouting from horizontal boreholes appears to be the most suitable method to emplace a continuous horizontal barrier. We determined that single injections are probably insufficient to effect a permeability reduction meeting barrier specifications, and that multiple injections are needed. Operational parameters have been identified, and a protocol for sequential injections has been designed.

5.2. Design Calculations

The emplacement of a horizontal grout-barrier beneath underground storage tanks is studied by means of numerical simulations. We have enhanced the capabilities of the TOUGH2™ code [*Pruess*, 1987,1991] to model grout injection and solidification. In our modeling approach, the chemical grout is treated as a miscible fluid the viscosity of which is a function of time and concentration of the gelling agent in the pore water.

If a certain high viscosity is reached and the movement of the injected grout plume ceases, the gel solidifies, leading to reduced porosity and permeability, increased capillary strength for a given water content, and a changed initial saturation distribution. The approach requires specifying a gel time curve, a mixing rule, and a solidification model which contains a permeability reduction model. The simulator is described in *Finsterle et al.* [1994*b*].

A two-dimensional vertical model was developed, and a heterogeneous, anisotropic permeability field was generated using simulated annealing techniques. The mean of the permeability field is 1.55×10^{-12} m^2 immediately beneath the tank, and 3.0×10^{-11} m^2 for backfill material [*Rockhold et al.*, 1992]. The standard deviation of the logarithm is assumed to be 1.0. The generated permeability field follows a spherical variogram with a horizontal and vertical correlation length of 6.0 and 1.0 meters, respectively.

The initial permeability field is illustrated in **Figure 5.1**. The parameters of van Genuchten's characteristic curves are taken from *Rockhold et al.* [1992], and the α parameters (see *Luckner et al.* [1989]) were adjusted according to Leverett's scaling rule, i.e. they are in inverse proportion to the square root of the permeability ratio.

We modeled multiple grout injections from two layers of horizontally drilled boreholes; the spacing between the wells is 1.0 meter. The layout of the wells is shown in **Figure 5.1**. Grout is injected at a rate of 12 kg per minute for an injection period of 1 hour. The chemistry of the grout is adjusted so that gel viscosity is doubled after 2 hours, and solidifies after 6 hours.

Figures 5.2, 5.3, and **5.4** show contours of grout content , i.e. the product of liquid saturation times grout concentration times porosity, between zero and 0.4 in 0.04 intervals. **Figures 5.2** and **5.3** depict the gel content after 50% and 100%, respectively, of the grout has been injected. Highest grout contents are in the immediate vicinity of the boreholes, were the initial soil gas and pore water is completely displaced due to the injection overpressure.

After redistribution of the plume due to gravity and capillary forces, however, maximum grout contents are encountered beneath the injection ports due to gravitational slumping of the plume (**Figure 5.4**). The relatively fast gelation (solidification occurs after 6 hours) prevents the plume from slumping down even further. Note that the spreading of the plume leads to an incomplete occupation of the pore space by grout, i.e. only partial plugging and insufficient permeability reduction will occur if only one injection is performed. After solidification of the gel, the porosity and permeability of the grouted region is reduced, leading to the permeability field shown in **Figure 5.5**.

Subsequently, a secondary injection is performed from the upper set of boreholes for 30 minutes. The grout from the secondary injection ponds on the low permeability layer produced by the primary injection (**Figure 5.6**), assuring high final grout saturations which guarantees that a continuous barrier of low permeability is formed. The porosity and permeability fields after solidification of the second plume are shown in **Figures 5.7** and **5.8**, respectively. It is evident that the upper grouted layer has very low porosities (0.015 or less), and the corresponding permeabilities are 10^{-17} m^2 or less (i.e. hydraulic conductivities of 10^{-8} cm/sec or less). These values confirm the theoretical containment ability of the barrier system under design.

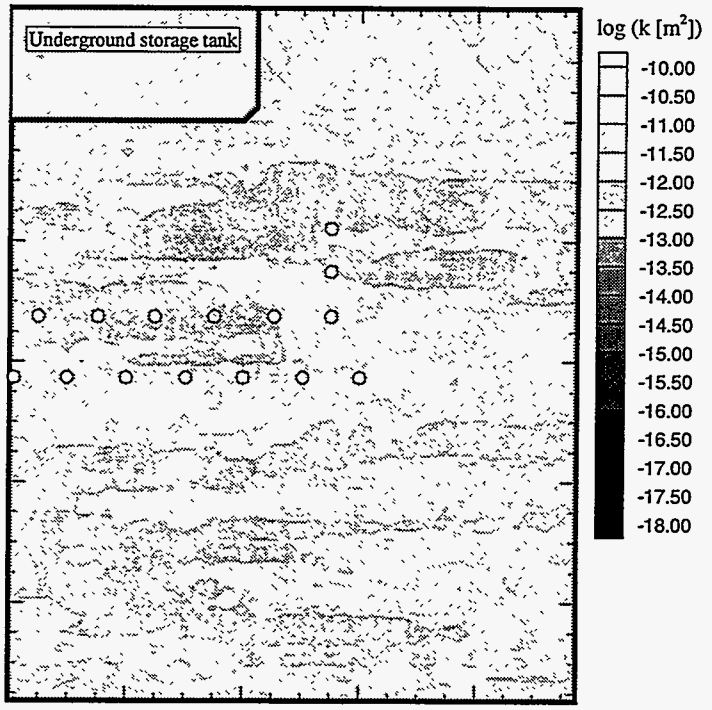

Figure 5.1. Model layout and initial permeability field.

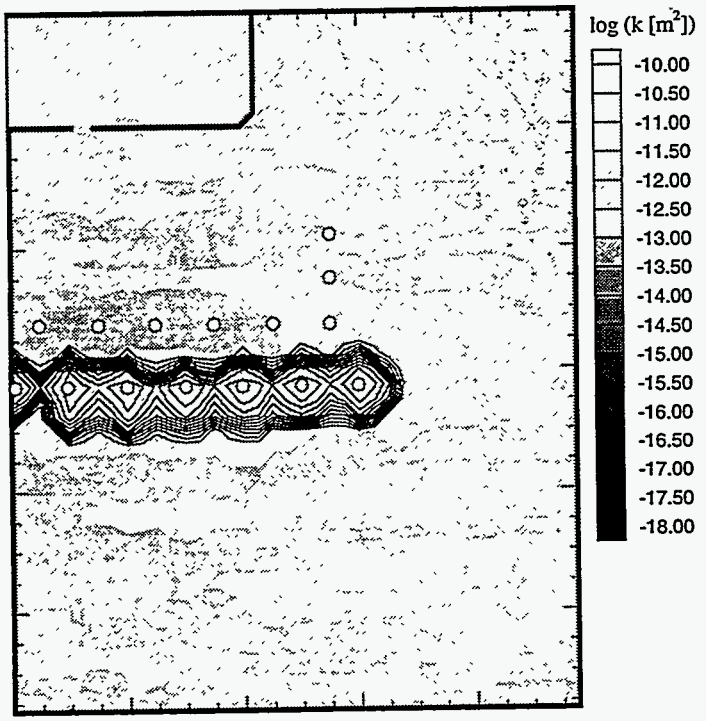

Figure 5.2. Initial permeability field (shaded) and gel content (contours) after 30 minutes of grout injection.

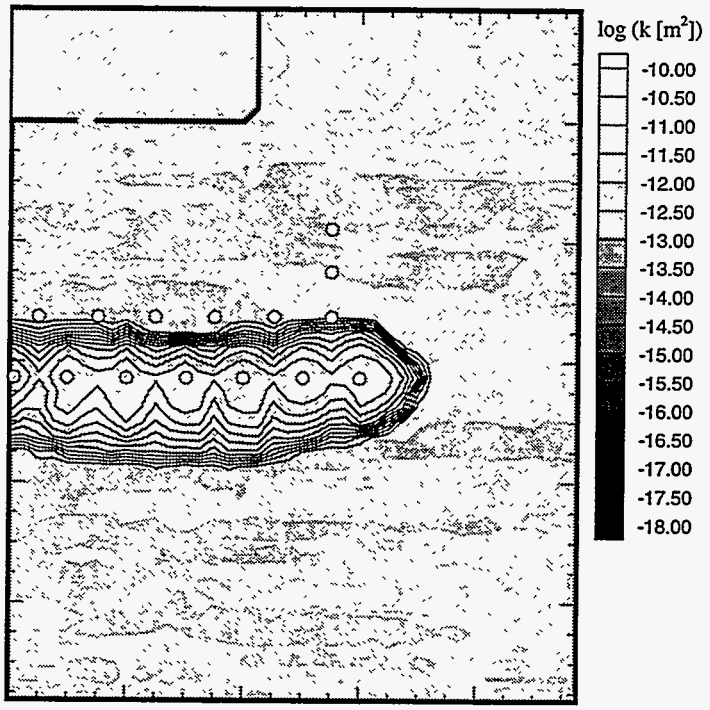

Figure 5.3. Initial permeability field (shaded) and gel content (contours) after 60 minutes of grout injection.

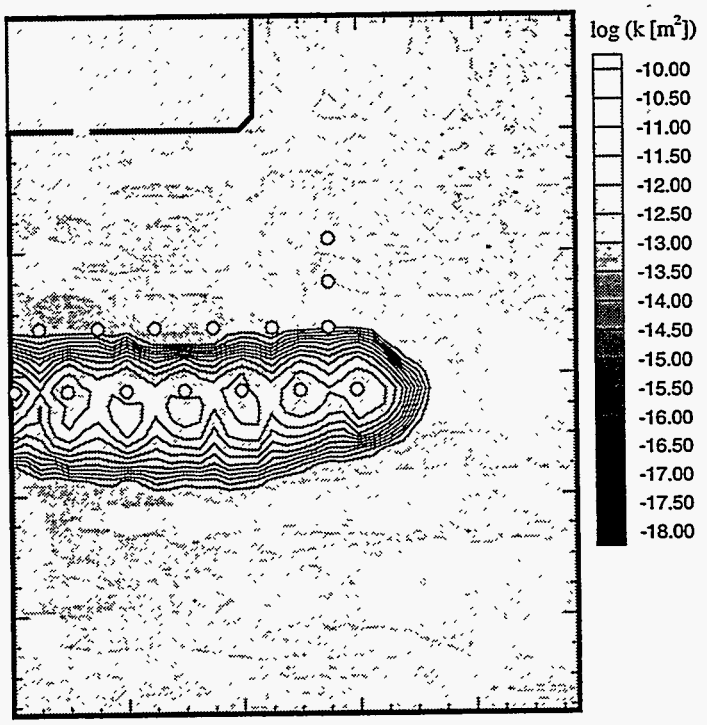

Figure 5.4. Initial permeability field (shaded) and gel content (contours) prior to solidification of primary grout plume.

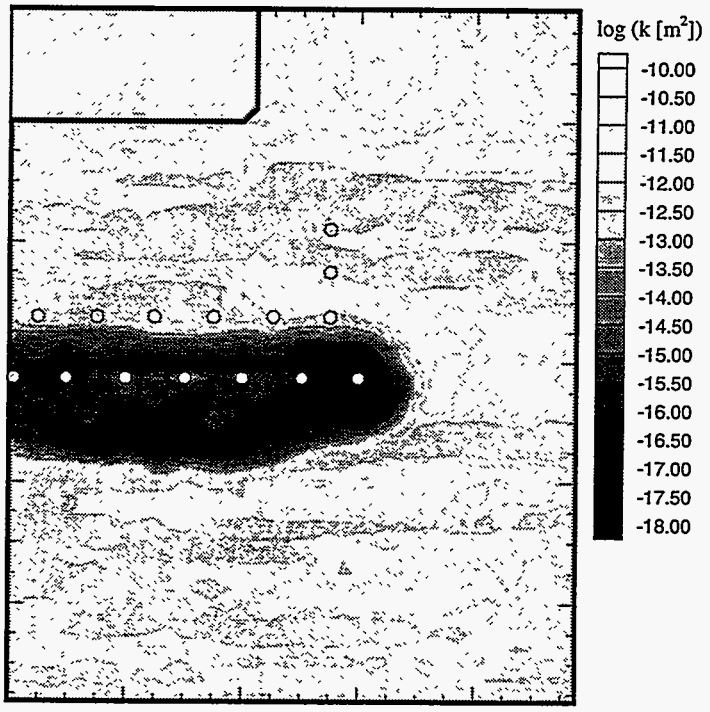

Figure 5.5. Permeability field after solidification of primary grout plume.

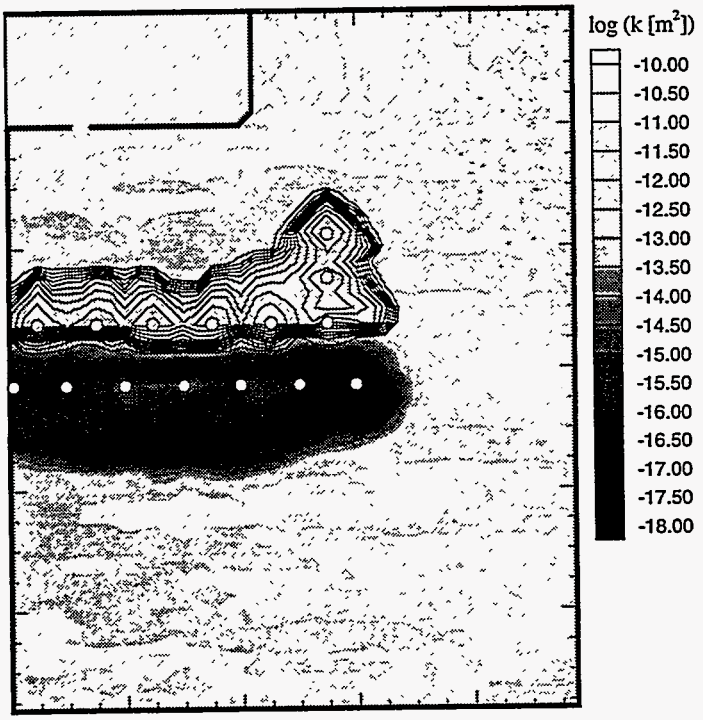

Figure 5.6. Permeability field (shaded) and gel content (contours) prior to solidification of secondary grout plume.

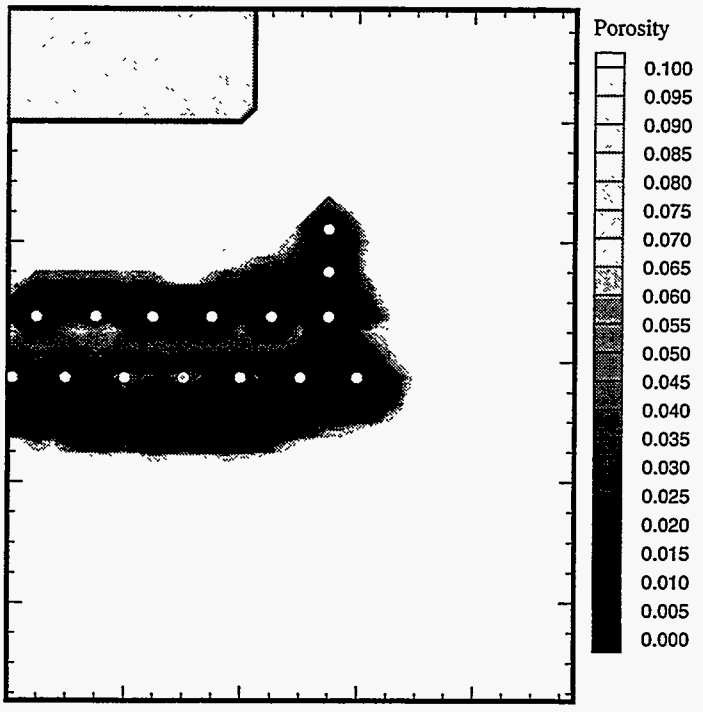

Figure 5.7. Porosity field after solidification of secondary grout plume.

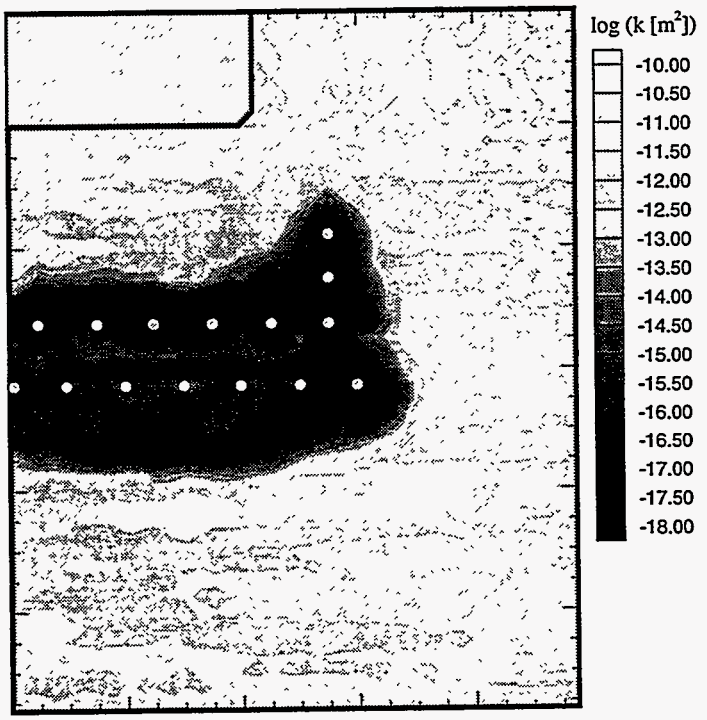

Figure 5.8. Permeability field after solidification of secondary grout plume.

5.2. Design of Monitoring System

The successful emplacement of the barrier as well as its integrity has to be assessed by post-emplacement testing and long-term monitoring. Prior to barrier emplacement, penetrometer measurements will be made to characterize soil conditions. Concurrently with injection, grouting pressure and volume injected will be observed, and surface displacements will be recorded with a network of tiltmeters and compared to the expected displacements predicted by model calculations.

After the injection is completed, penetrometer measurements will be repeated, and soil samples are taken at selected locations. The presence of potential holes in the barrier may be detected using seismic imaging techniques, hydraulic pressure tests, or liquid and gas tracer tests. Finally, a long-term monitoring system will be installed to control contaminant concentrations above and below the grout barrier.

The data can be compared to model predictions. A protocol for potential remediation strategies will be developed in the case of a barrier failure. **Figures 5.9** and **5.10** show the simulation of a tank leak, and how the released contaminant ponds on top of the subsurface barrier. Note that **Figure 5.10** corresponds to a time of 48 hrs from the beginning of leaking at a rate of 0.02 kg/sec, i.e. when a total of 3500 kg of contaminated water has leaked from the tank. No flow of the contaminants through the barrier is observed, which is a clear indication of barrier impermeability.

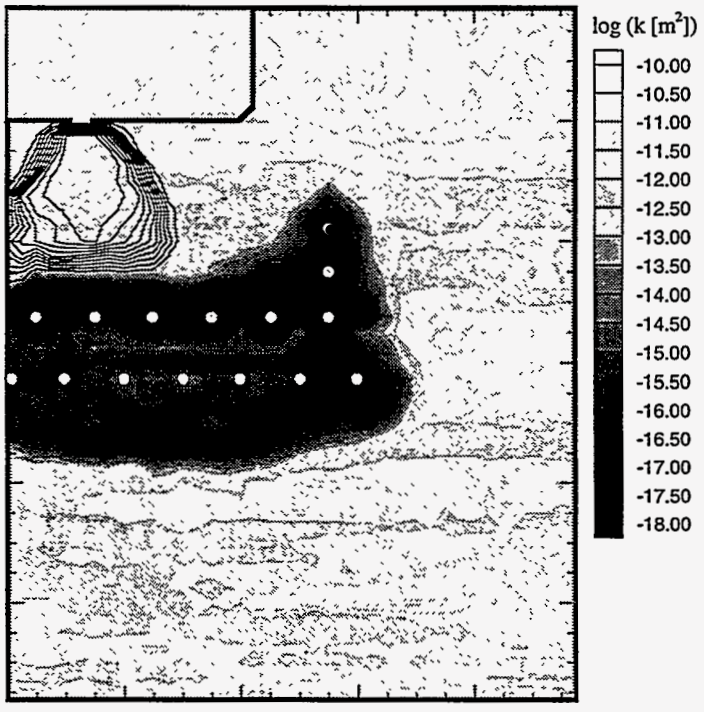

Figure 5.9. Simulation of leaking tank with barrier in place.

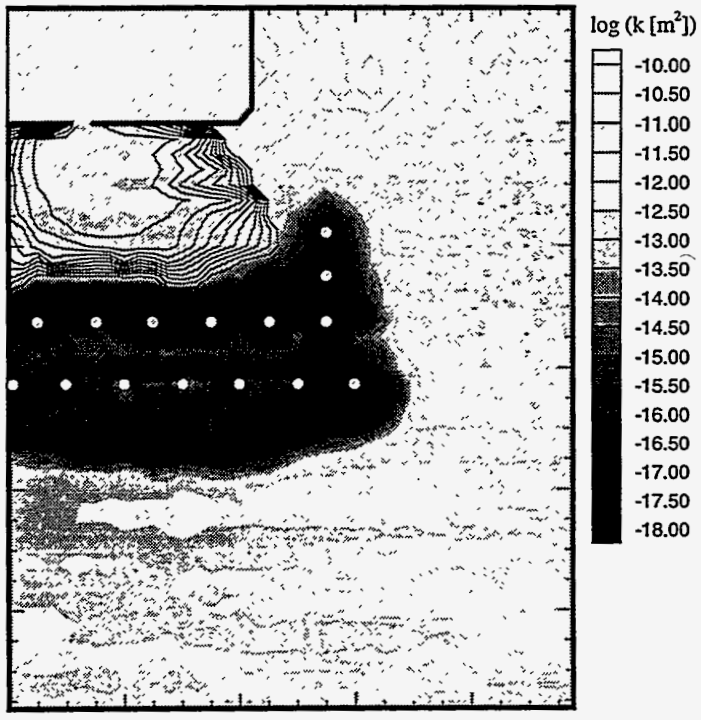

Figure 5.10. Containment of contaminant by subsurface barrier.

6. ENGINEERING DESIGN

In this section we discuss the engineering design of the medium-scale field demonstration. Specifications for the injection and monitoring aspects of the field test are set, and engineering drawings are presented.

6.1. Drilling

The test field will be located at the edge of a 20 foot high berm for convenience (Figure **6.1**). This will permit horizontal drilling access to the test field. The materials consist of an alluvial deposit underlying a three to four foot thick layer of residual soil. The alluvium is composed of sand, silt, gravel, clay with occasional cobbles (see Section 4). The entire deposit is stratified and generally heterogeneous.

The drill hole pattern will consist of two horizontal rows of holes as shown in **Figures 6.2, 6.3**, and **6.4**. The rows have a five foot vertical separation (**Figure 6.3**) and a five foot lateral hole-to-hole spacing (**Figure 6.2**). The crosshatched regions in **Figures 6.2** show the idealized areal extent of the injected grout. The boundary of this region is set back about 15 feet from the face of the berm. The holes will be angled down at five degrees from the horizontal for ease of installation (**Figure 6.4**). Grout will be injected from ports along the length of the hole as shown in Figure 3.

Drilling equipment will be located at the base of the bench. Holes will be advanced with rotary percussion and/or casing advancer methods. Casing advancer drilling equipment is shown in **Figure 6.5**. The drilling method will be required to penetrate cobbles and incorporate cement-bentonite slurry circulation. Hole deviation will not exceed one foot at any point along the advance. A drill collar set at the beginning of the hole and extending from the face will help to minimize hole deviation. Borehole surveys, using a single shot downhole camera or equivalent, will be carried out.

The completed drill holes will be installed with a sleeve-port-grout-pipe (SPGP). Details of the standard SPGP, used if access to the hole is not required for seismic testing, are shown in **Figure 6.6**.

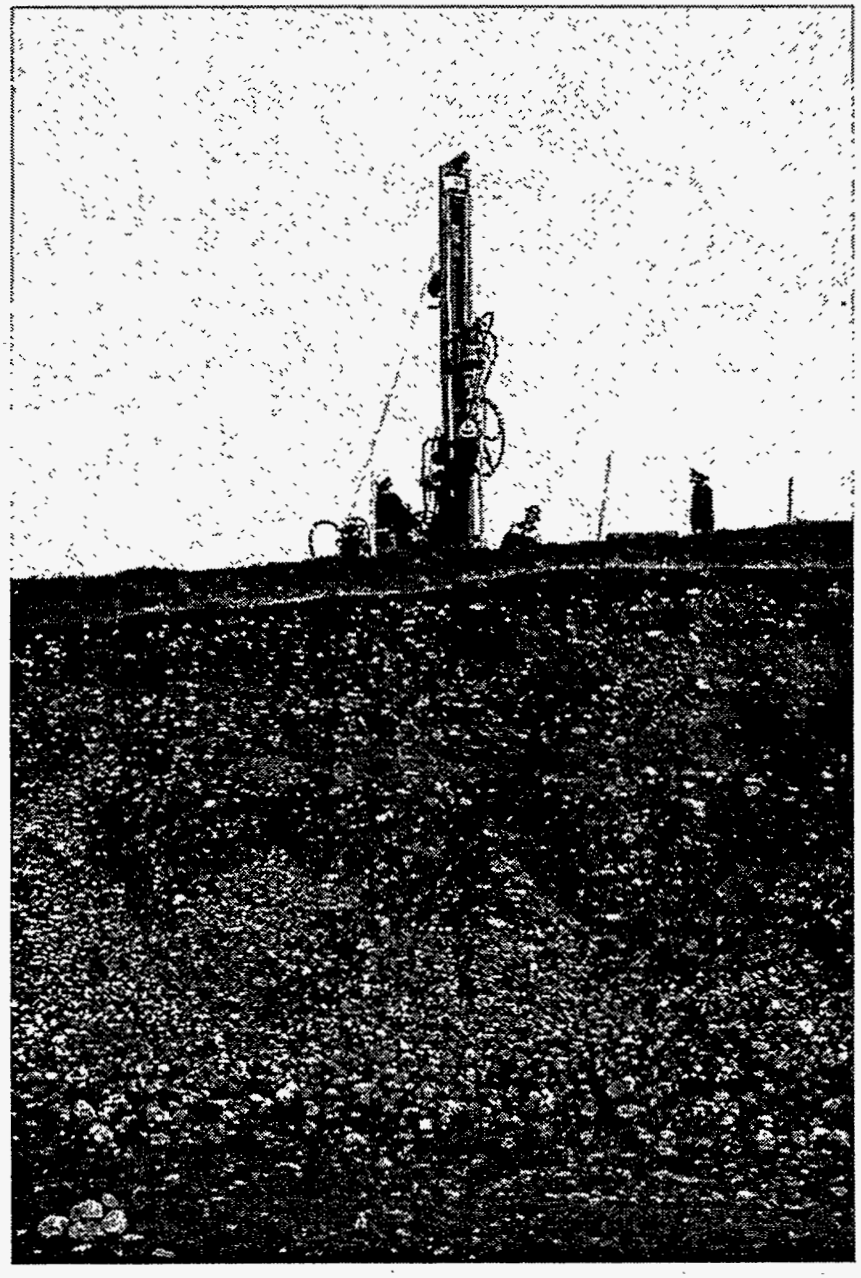

Figure 6.1. The 20-foot high berm at the test pad site.

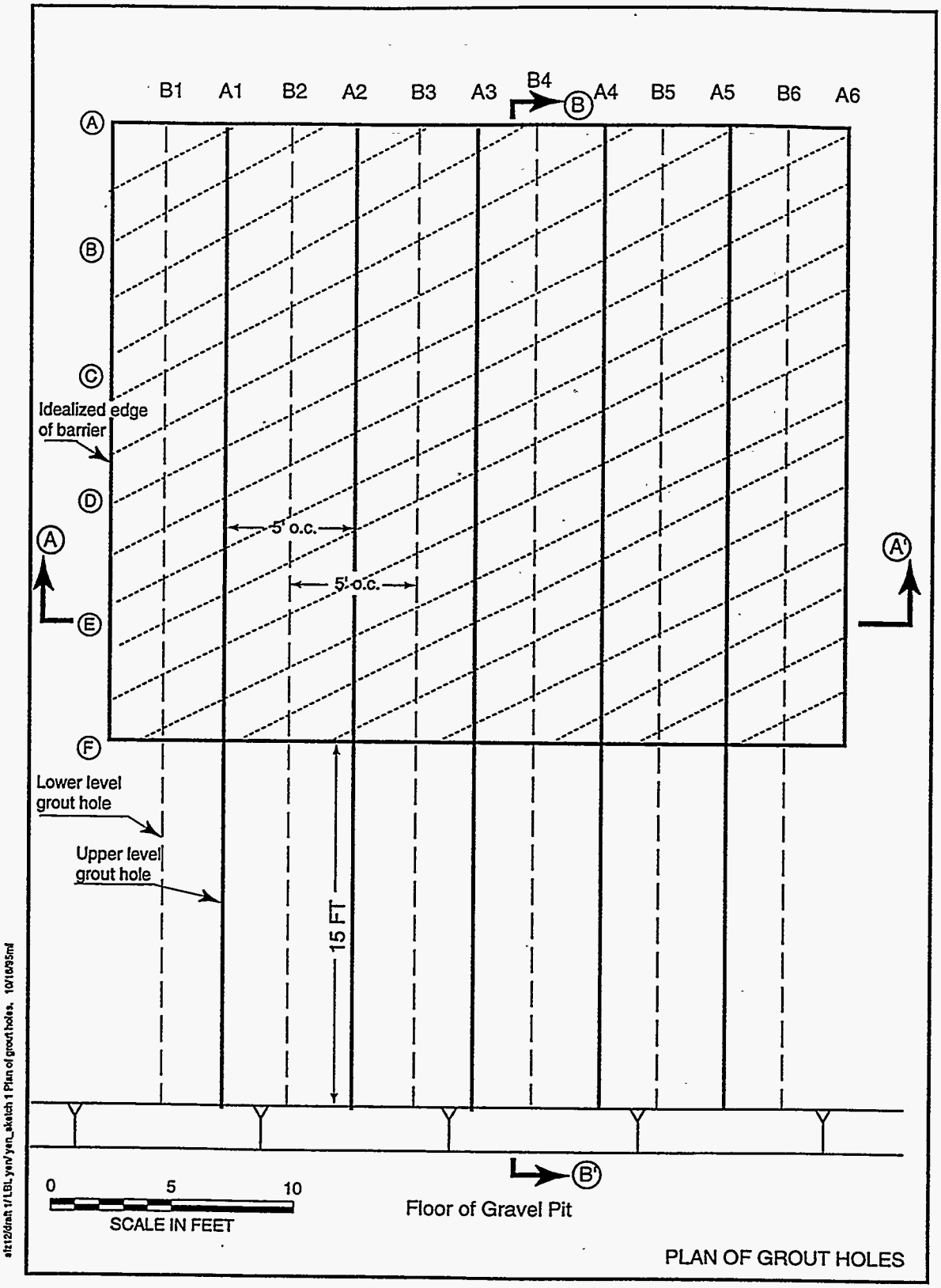

Figure 6.2. Plan of grout holes.

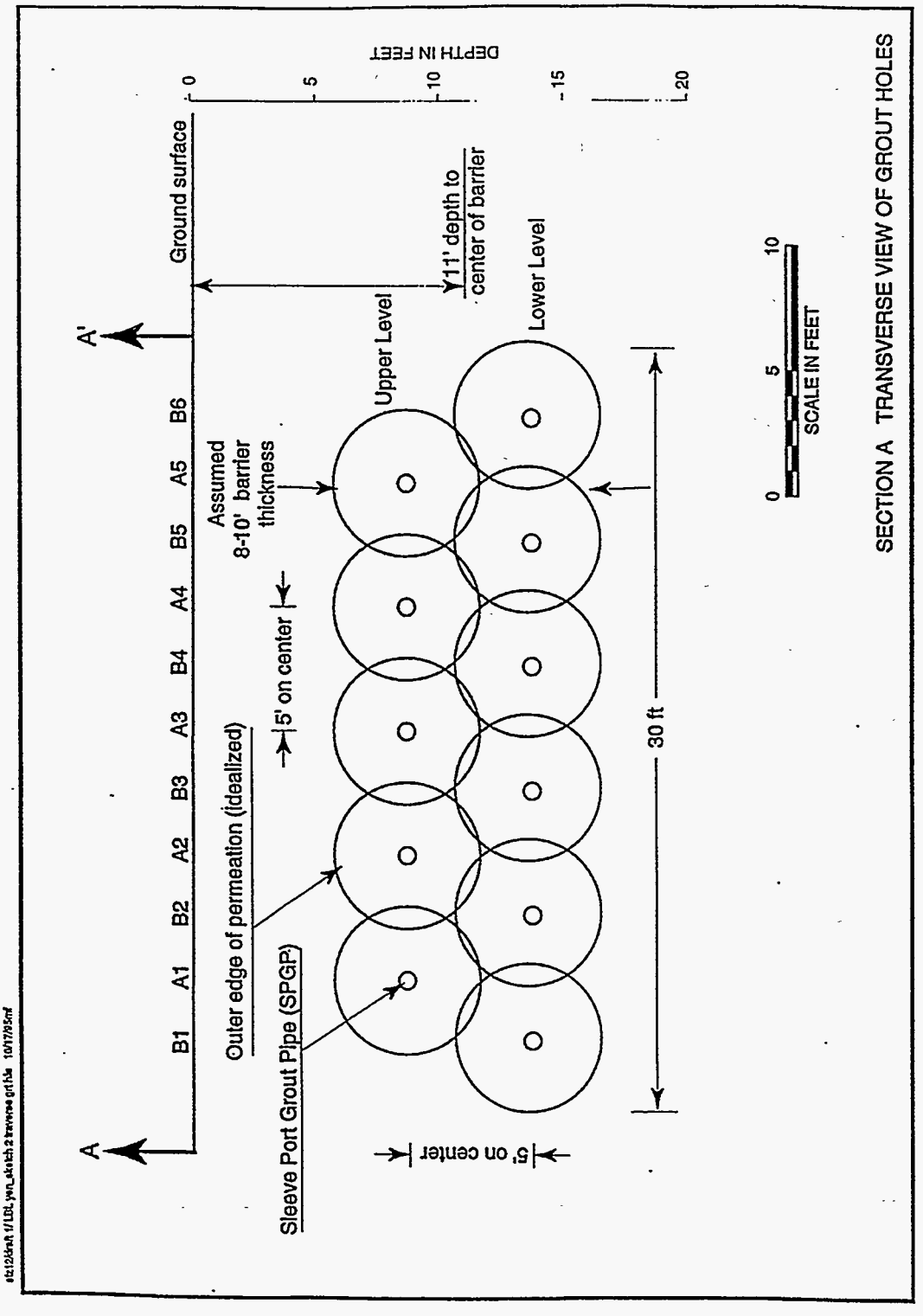

Figure 6.3. Transverse view of grout holes.

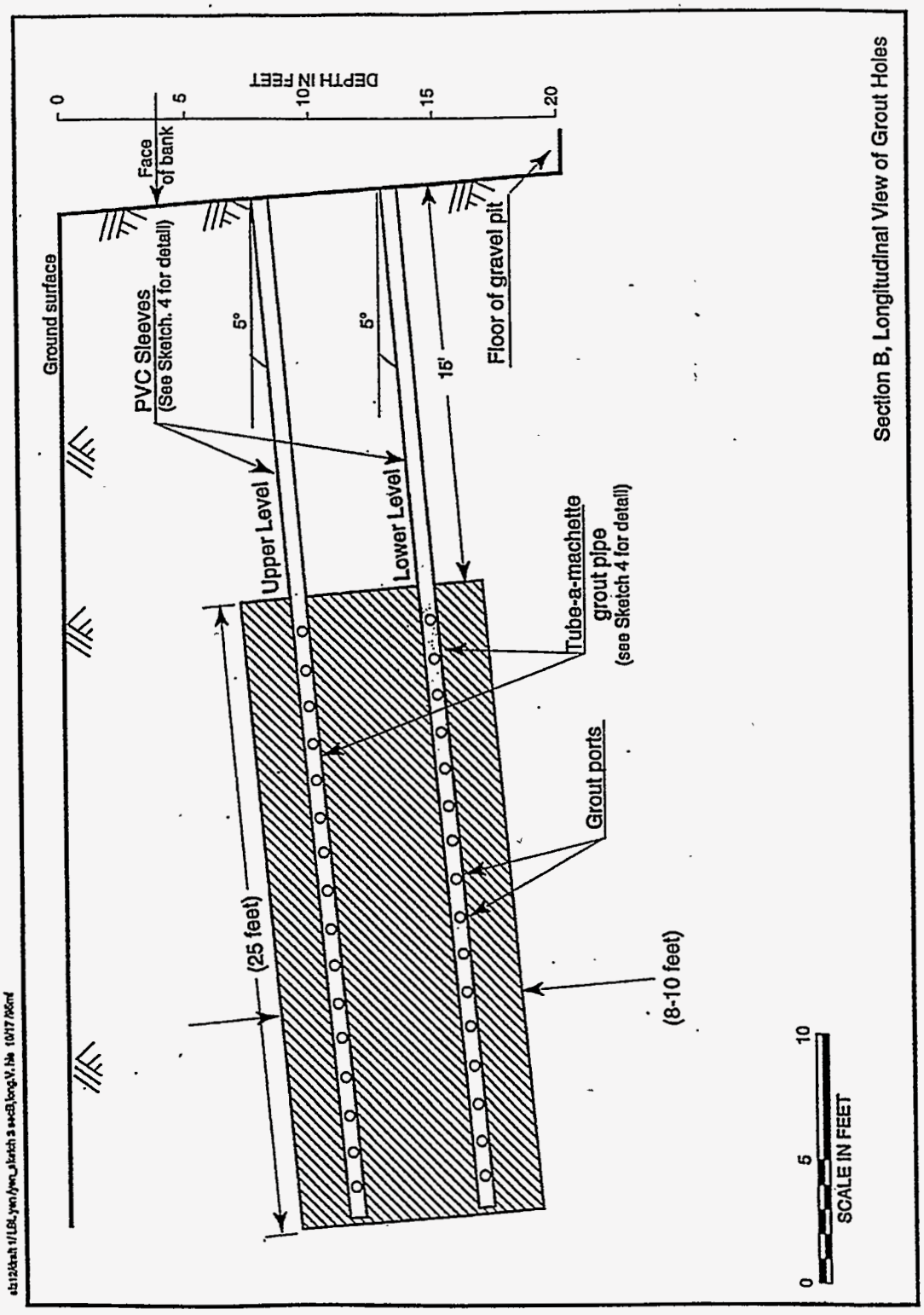

Figure 6.4. Longitudinal view of grout holes.

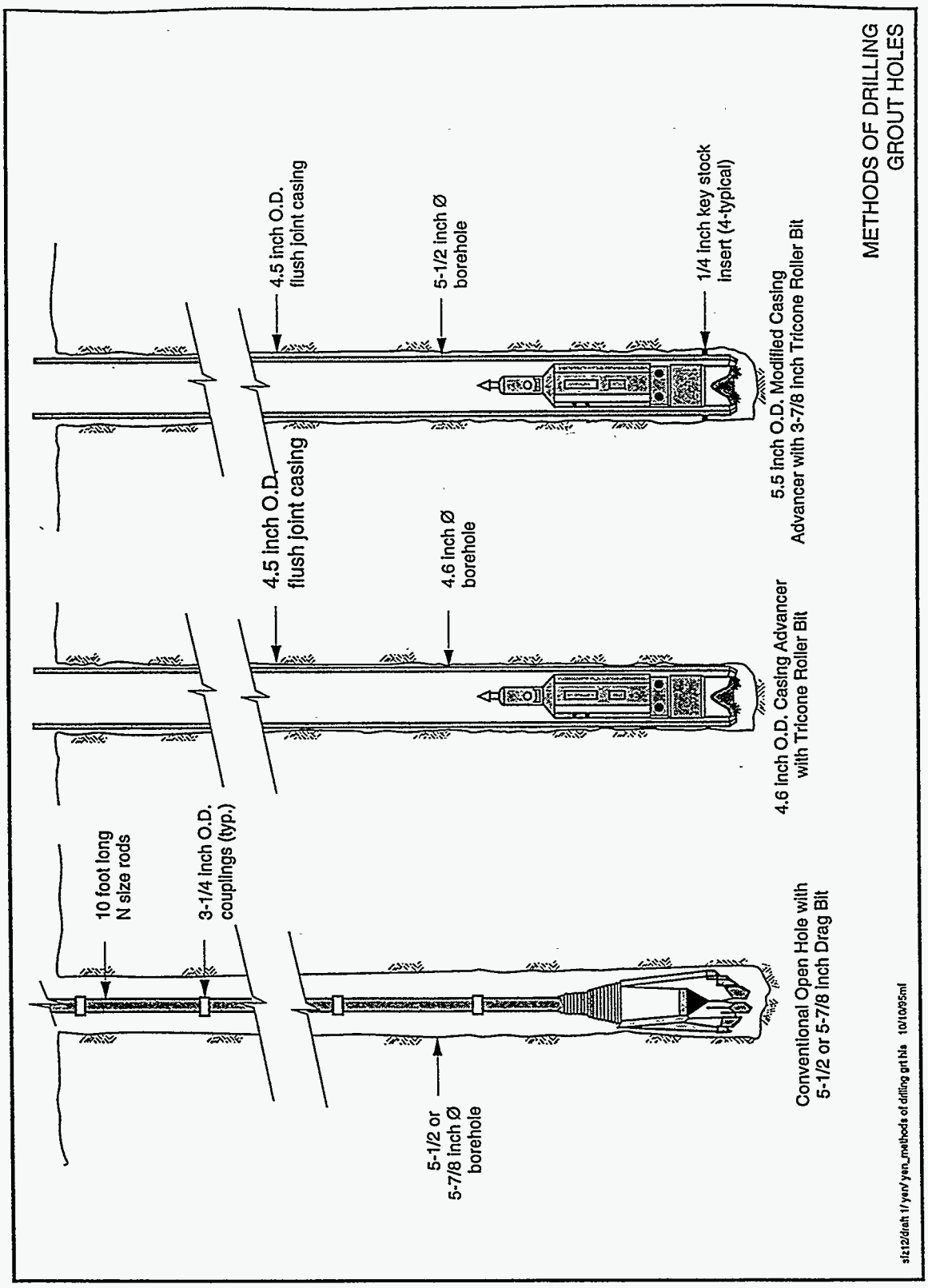

Figure 6.5. Potential methods for drilling the grout holes.

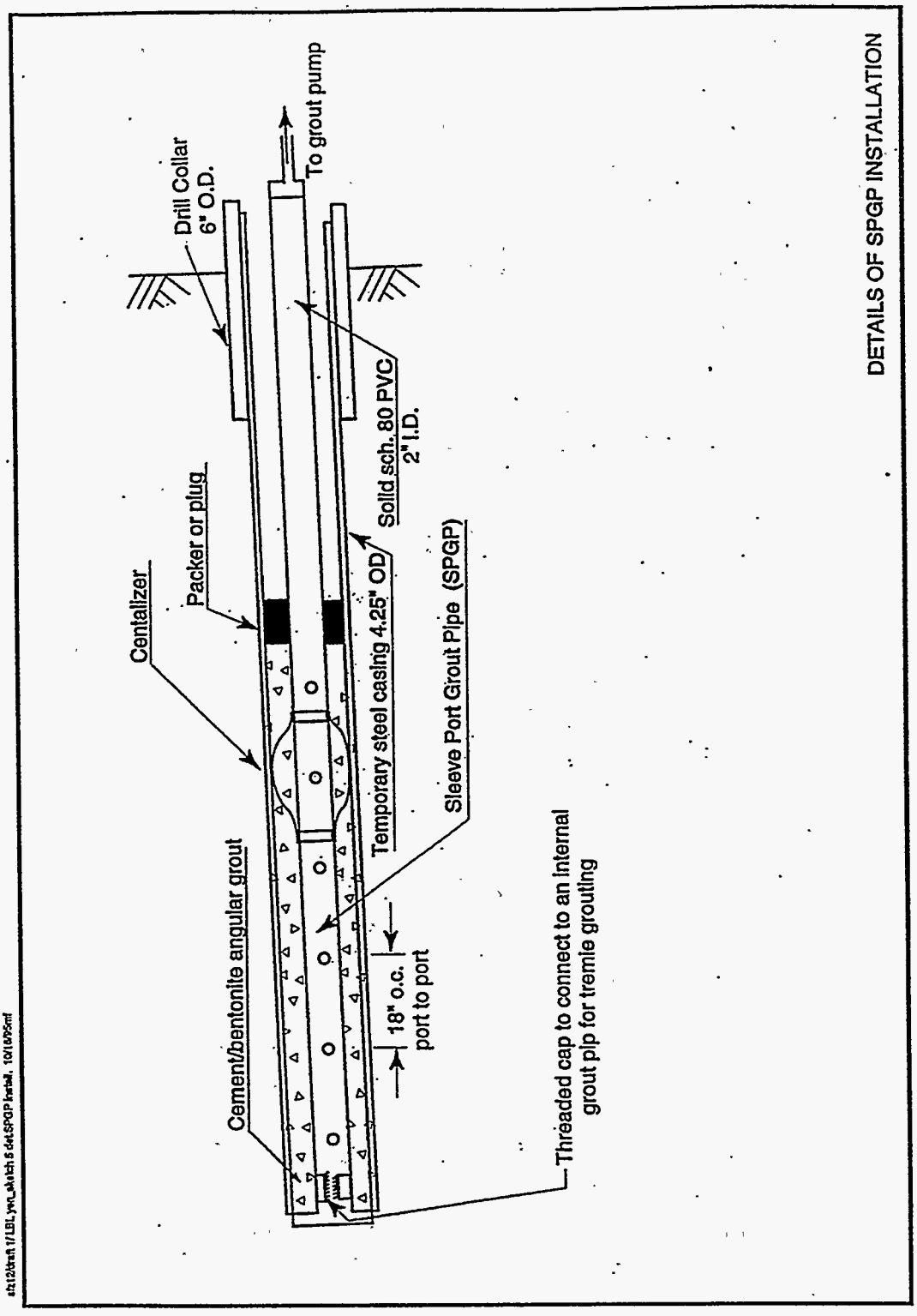

Figure 6.6. Details of the SPGP installation.

The SPGP will be constructed of 2" diameter Schedule 80 PVC, fitted with grout ports at 1.5 feet intervals. Centralizers will be installed at 6 foot intervals. The tip of each SPGP will have a fitting to receive a temporary grout pipe.

After the SPGP is installed, it will be tremie grouted during the removal of temporary casing. The packer shown in **Figure 6.6** is provided so that the tremie grouting can be conducted under a small pressure. The combination of rotary drilling, cement-bentonite slurry circulation, and tremie grouting is carried out to assure an intimate contact between the cement grout outside and SPGP and the formation. This intimate contact is required so that a preferential flow path for the chemical grout is not formed at the interface between the cement grout and the formation.

In order to permit access for seismic measurements a modified SPGP installation is shown in **Figure 6.7**. The modified SPGP incorporates a larger diameter PVC tube. Use of a larger diameter tube also minimizes the annular space between the tube and the formation. This helps to maintain formation integrity by minimizing the amount of material which can fall into the hole.

6.2. Grout Injection Sequence

The sequence of injection is shown in **Figure 6.8**. In general, the lower level of holes will be grouted prior to the upper level. The objective is to concentrate the grout flow to the desired location. The injection sequence is as follows:

(a) The ports at the boundary of the test field will be injected first. This includes the full depth ports, collar ports and end pipes of each level. Alternating holes will be injected in a primary and secondary sequence.

(b) The test field will be subdivided by grouting selected ports, thereby forming the boundaries of internal cells.

(c) Ports within cells will be injected.

(d) Cells will be completed in a checkerboard fashion (primary-secondary) along alternating rows.

(e) Alternating ports will be injected in each individual pipe, in an alternating primary-secondary sequence, or primary-secondary-tertiary sequence.

(f) The upper level holes are injected after all grouting in the lower level are completed.

(g) The upper level injection sequence (rows, cells and ports) will be staggered in plan from that in the lower level.

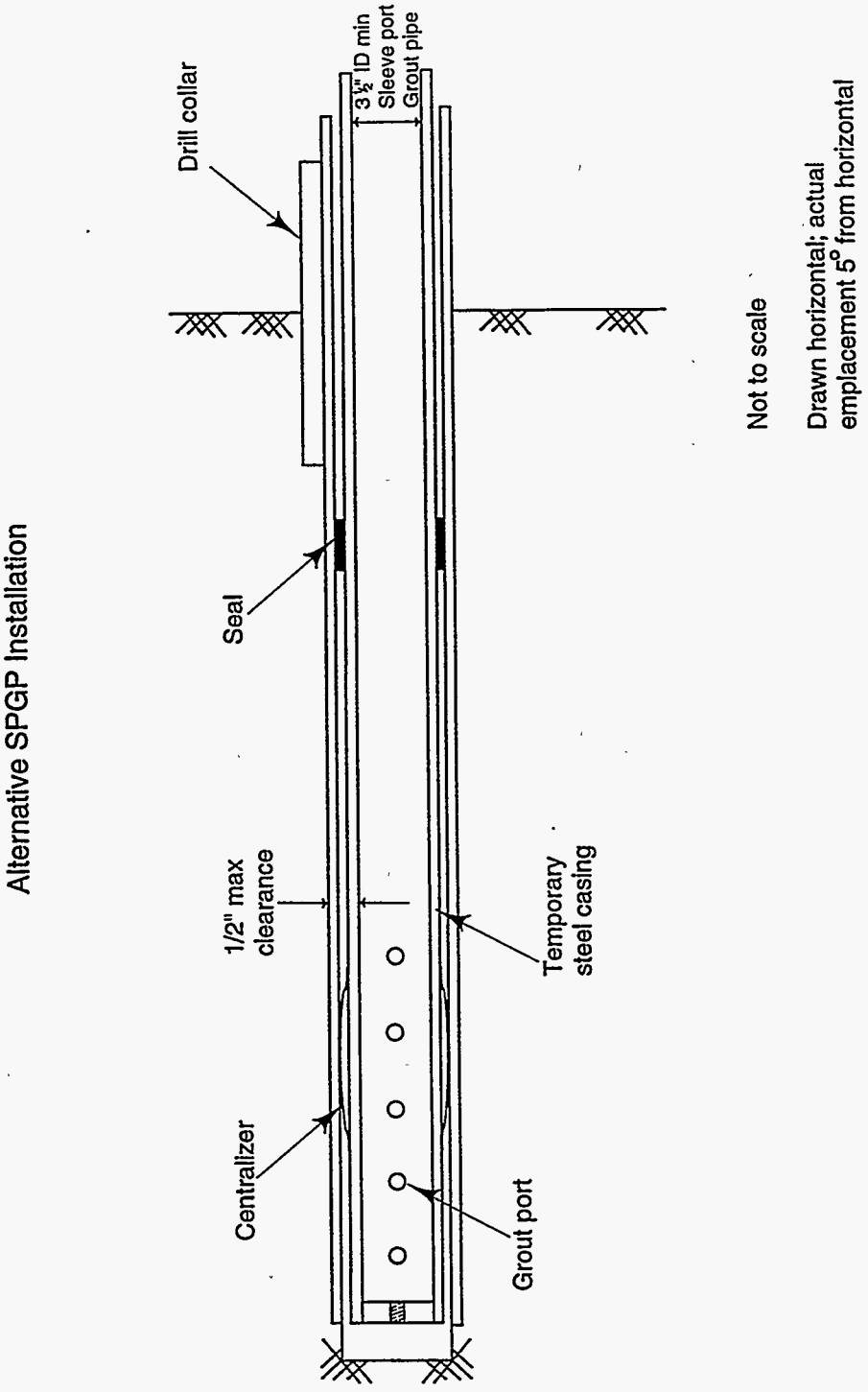

Figure 6.7. Alternative SPGP installation.

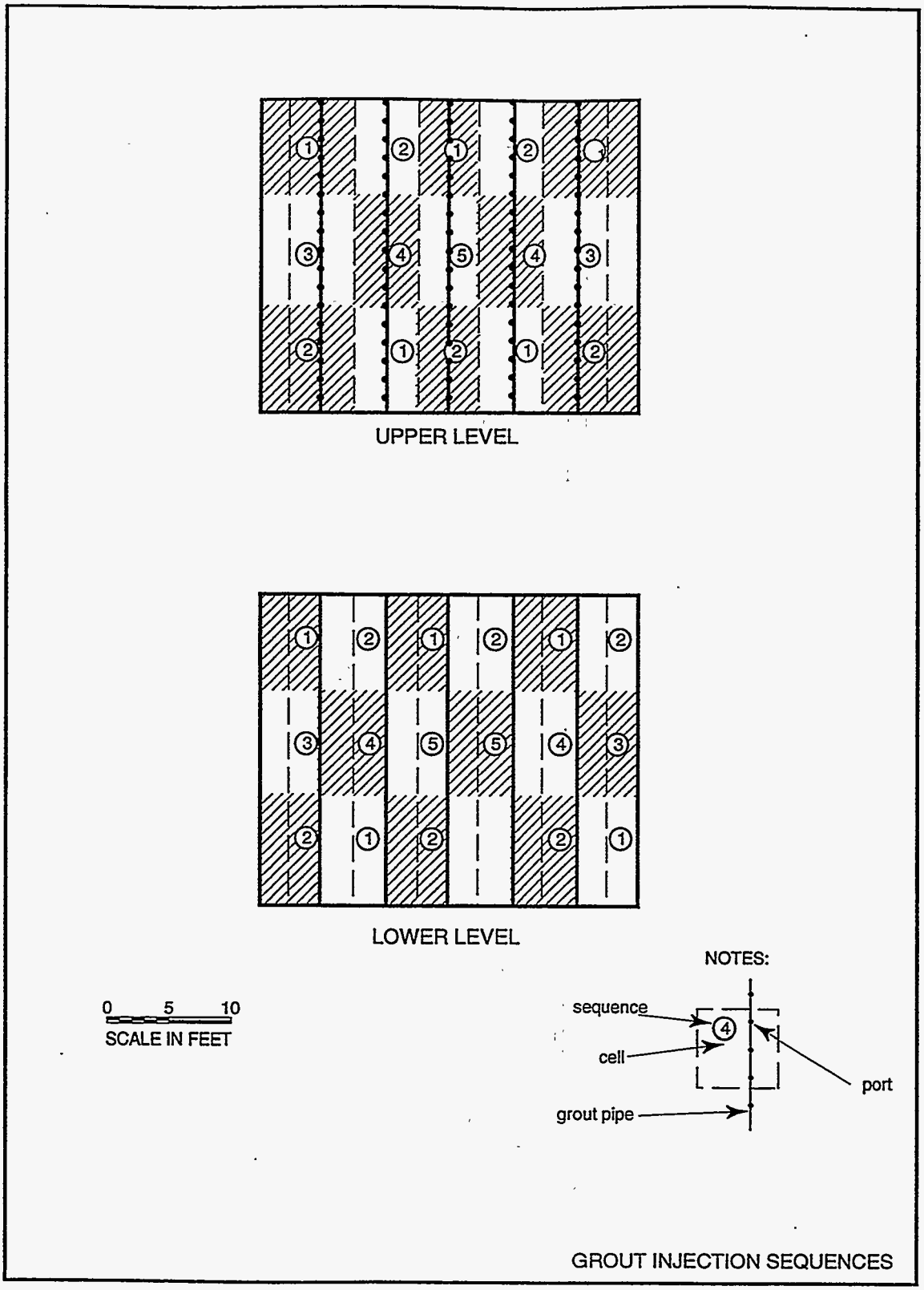

Figure 6.8. Grout injection sequences.

6.3. Instrumentation for Injection and Monitoring

The tiltmeter array is shown in **Figure 6.9**. A total of 23 instruments will be installed prior to grouting. Borehole tiltmeters will be used to measure incremental ground motions caused by grouting. Tiltmeter output will be monitored during grouting operations. Data will be stored on computer and analyzed after the test to model the shape and extent of the grout barrier.

Grout take per hole and per port will be monitored using electronic flow meters and grout pressure transducers. Data will be electronically recorded on dataloggers and will be downloaded into computers, providing real time information for analysis and control.

Air permeability testing will be conducted before and after grout injection. An array of 11 holes will be required as shown schematically in **Figure 6.10**. Nine holes will be drilled from the top of the bench to a nominal depth of 7 feet. These holes will be drilled using the ODEX system (**Figure 6.11**). Casing is advanced with the bit and chips are removed pneumatically. After the hole is drilled, a 2" OD PVC tube is placed in the hole. The annular space is filled with bentonite pellets for a seal.

Two horizontal holes will be drilled from the base of the bench, beneath the horizontal grout barrier, utilizing the hole drilling method described above for grout holes. Holes will be inclined downward five degrees from the horizontal and will be surveyed. The holes will be completed using 2 inch diameter, scheduled 40 PVC installed and tremie grouted as described above. After the grout has set a drill rod will be pushed down the PVC tube and the hole extended for 1 to 2 feet beyond the end of the tube.

The barrier verification involves both direct and indirect methods. Direct methods measure directly the parameter of interest, i.e. the permeability of the grouted formation, and include hydraulic, pneumatic, and tracer techniques. Indirect methods are based on geophysical measurement; these do not provide permeability measurements but allow the non-intrusive determination of the barrier extent, geometry and continuity. A detailed discussion of direct and indirect methods for barrier verification and evaluation can be found in a companion report [*Moridis et al.*, 1995c]. In this section we present only limited information which has implications for the design and layout of the field demonstration.

Seismic geophysical surveying will be conducted between the holes within the barrier prior to and after grout injection. Comparison of results will provide information on the continuity and integrity of the barrier. A piezoelectric source will be used to generate seismic waves which will be received in other boreholes as shown schematically in **Figure 6.12**. The source borehole will be filled with water to provide signal coupling. Data will be recorded by computer and stored for analysis. Multiple source receiver points will provide dense ray coverage.

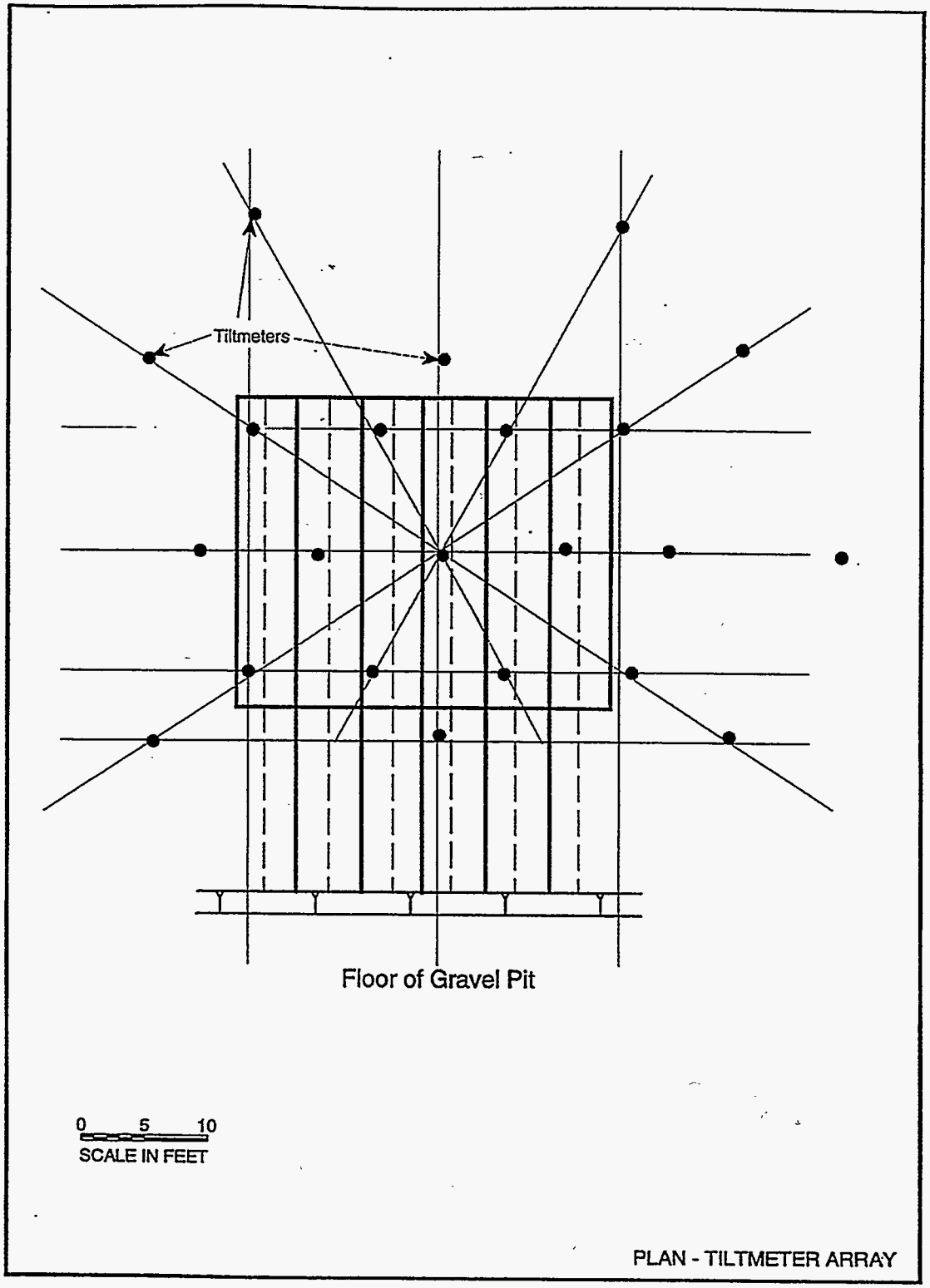

Figure 6.9. Layout of the tiltmeter array.

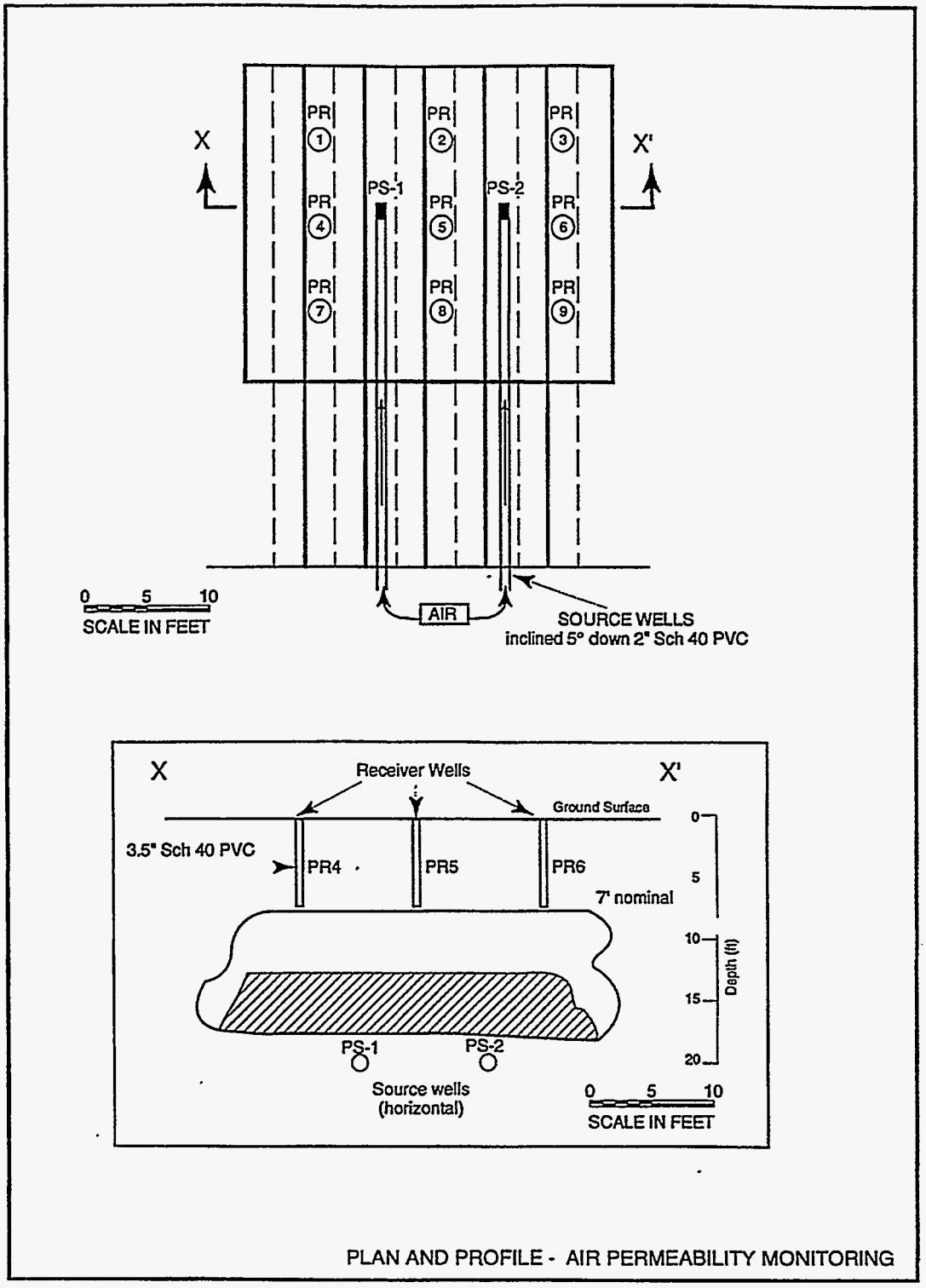

Figure 6.10. Layout of the air-permeability system for barrier testing.

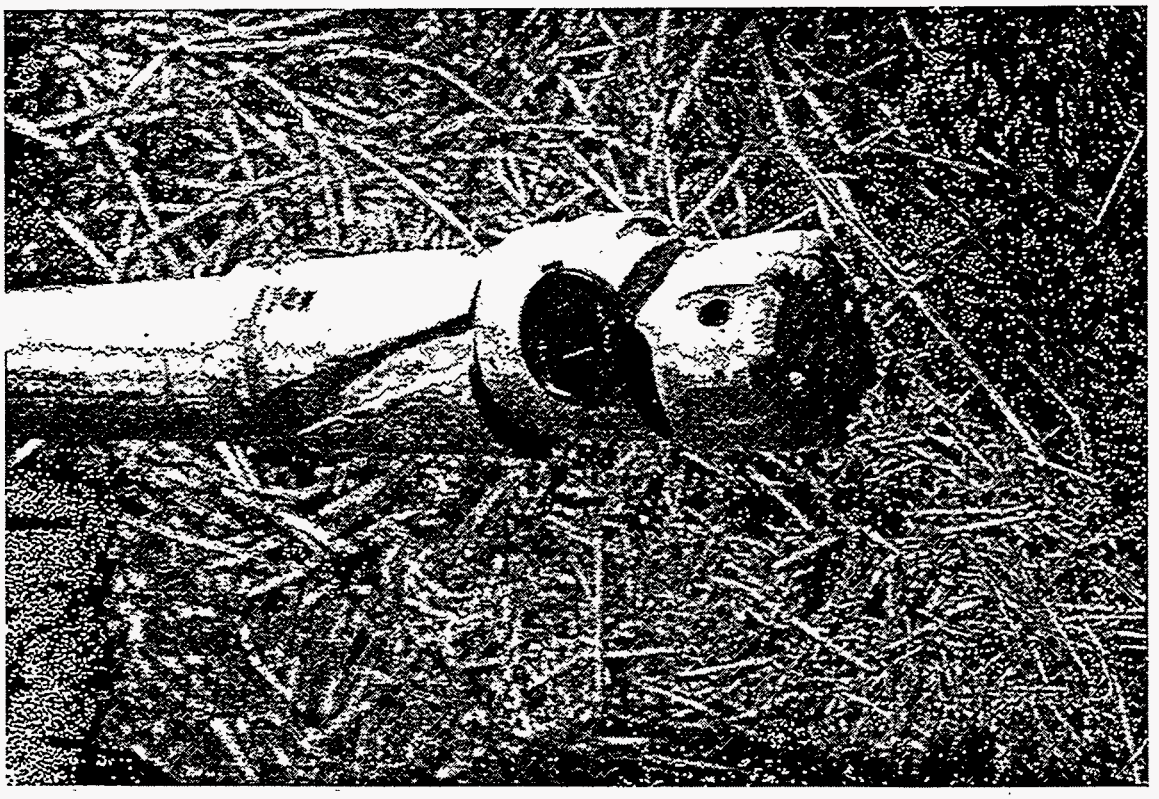

Figure 6.11. Close-up of ODEX kit.

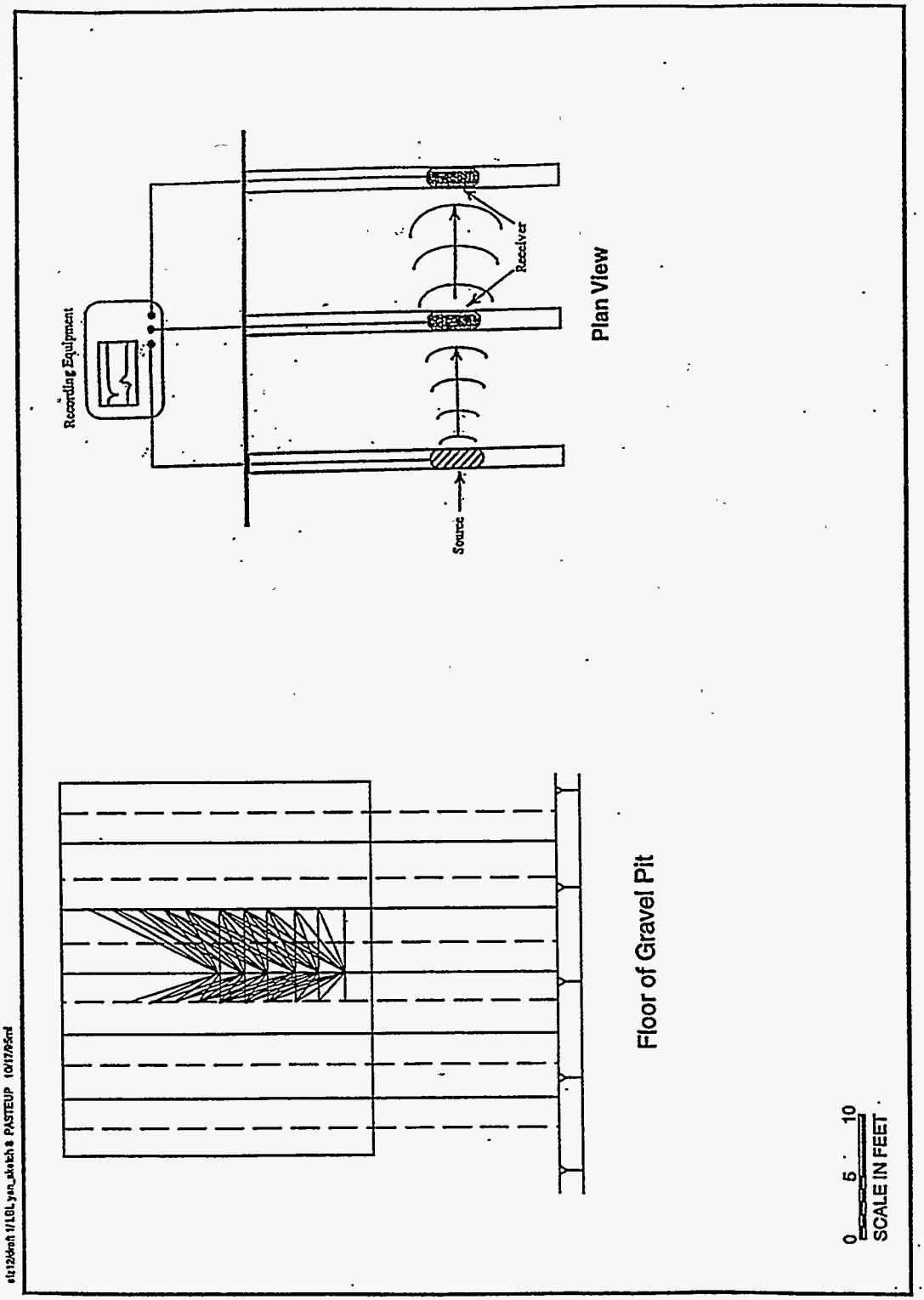

Figure 6.12. Layout of the seismic investigation array.

Figure 6.12 illustrates a portion of the ray coverage for the survey. This pattern will be repeated over the entire barrier volume.

Ground penetrating radar testing will be conducted in selected boreholes. GPR probes will be inserted and will provide data on the degree of signal attenuation obtained due to presence of grout. The details of this test are under consideration and a sketch has not been prepared.

Electrical resistivity is also being considered as another technique for measuring grouting continuity in conjunction with post grouting permeability tests. The details of this test are under consideration and a sketch has not been prepared.

6.4. Post-Injection Excavation and Sampling

Depending on available budget, a test excavation will be made to reveal the grouted materials in situ. Samples of grouted and ungrouted materials will be taken for testing. The test excavation will be logged and photographed. Measurements will be made of drilling accuracy and notes will be taken of the completeness of permeation in the subsurface materials.

Two alternative excavation places are shown in **Figures 6.13** and **6.14**. The "maximum excavation" alternative involves exposure of the entire barrier by removal of material above and around it. The "minimum excavation" alternative involves exposure of a portion of the barrier via excavation of a slot.

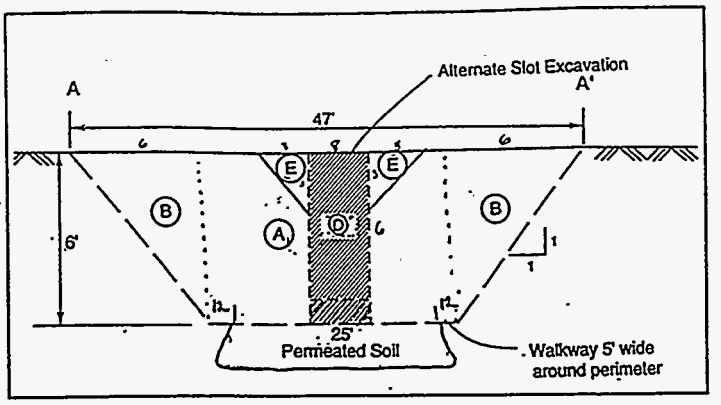

SCHEMATIC TEST EXCAVATION CROSS-SECTION

Calculation of Volume - Submass Excavation

Volume (A) (WxLxH)	49' x 45' x 6' = 13,230 ft^3	= 490 yd^3
Volume (B)	6' x 6' x 45' = 1620 ft^3	= 60 yd^3
Volume (C)	6' x 6' x 17.5' = 630 ft^3	= 23 yd^3
		573 yd^3 total mass excavation

Calculation of Volume - Submass Alternate

Volume (D) (WXLXH)	8' x 6' x 45' = 2160 ft^3	= 80 yd^3
Volume (E)	3 x 3' x 45' = .405 ft^3	= 15 yd^3
		95 yd^3 total alternate slot excavation

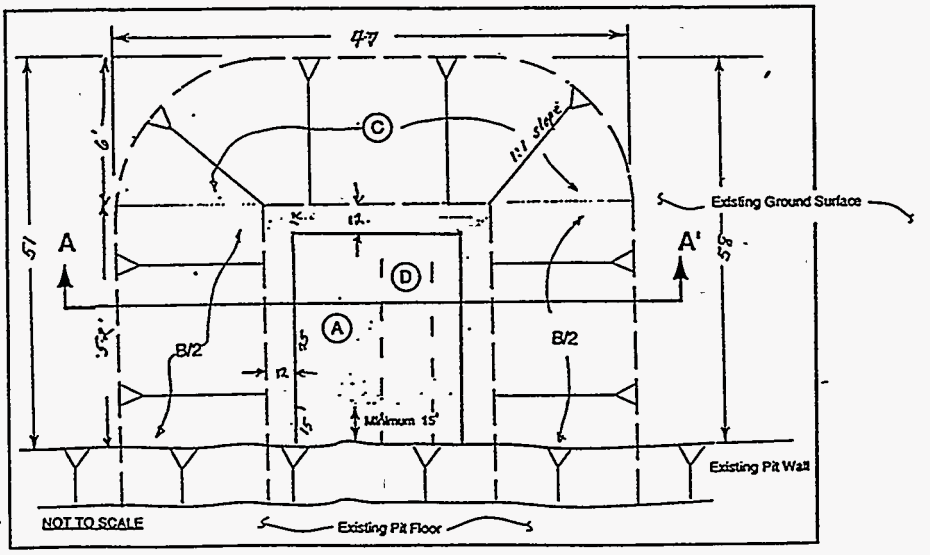

MAXIMUM EXCAVATION

sh12/dnh 1/yen/yen_sketch 10-max.excav. 10/11/95mf

Figure 6.13. Minimum excavation option.

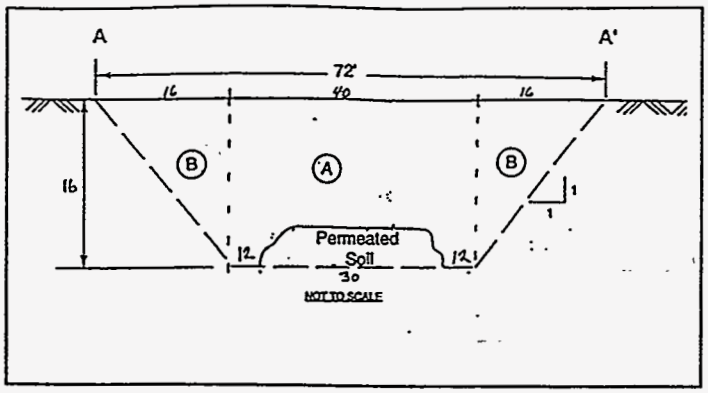

SCHEMATIC TEST EXCAVATION CROSS-SECTION

Calculation of Volume - Submass Excavation

Volume (A) (WxLxH) $54' \times 45' \times 16' = 38{,}880\ ft^3 = 1440\ yd^3$

Volume (B) $16' \times 16' \times 45' = 11{,}520\ ft^3 = 427\ yd^3$

Volume (C) $16' \times 16' \times 17.5' = 4{,}480\ ft^3 = 166\ yd^3$

$2033\ yd^3$

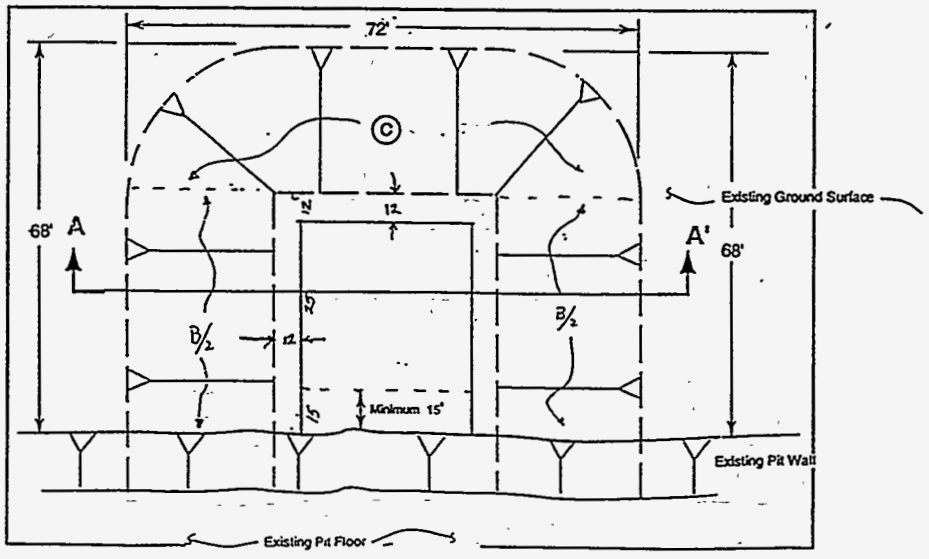

MAXIMUM EXCAVATION

Figure 6.14. Maximum excavation option.

7. SUMMARY

This report is the design study for a medium-scale field demonstration of LBNL's new subsurface containment technology for waste isolation using a new generation of barrier liquids. The test site is located in central California in a quarry owned by the Los Banos Gravel Company in Los Banos, California, in heterogeneous unsaturated deposits of sand, silt, and gravel typical of many of the arid DOE cleanup sites and particularly analogous to the Hanford site. This effort is part of the project *Containment of Contaminants Through Physical Barriers Formed From Viscous Liquids Emplaced Under Controlled Viscosity Conditions.*

The current phase of the project involves the second field test of the LBNL viscous barrier technology, and represents a scale-up from the first small-scale field test conducted in January 1995 [*Moridis et al.*, 1995*a*; 1995*b*]. The goals of the current phase of this project are:

(a) To demonstrate the ability to create a continuous subsurface barrier isolating a medium-scale volume (30 ft long by 30 ft wide by 20 ft deep, i.e. 1/10th to 1/8th the size of a buried tank at the Hanford Reservation) in the subsurface.

(b) To demonstrate the continuity, performance, and integrity of the barrier.

Section 1 provides a brief project description and overview, states the objectives of this effort, and provides background information on the LBNL subsurface barrier technology.

In Section 2 we discuss the preparatory supporting work that provided the necessary information for the design planning of the medium-level field demonstration of the LBNL barrier fluid technology. The preparatory work discussed here includes (a) the identification and characterization of promising materials, (b) the evaluation of their containment potential by means of laboratory and pilot-scale experiments, (c) the development of predictive capabilities for the study of a number of alternative injection scenarios through numerical simulation, (d) the interactions with industry, academia, and regulatory agencies, as well as (e)

the design and successful execution of the first-level field demonstration of the LBNL containment technology.

Section 3 is devoted to the barrier liquids to be used in the medium-scale field demonstration. Two barrier liquids are under consideration: **C**olloidal **S**ilica (CS) and **P**oly**S**ilo**X**ane (PSX). The gelation behavior of these materials is discussed in detail. PSX exhibits slight and/or controllable effect of the soil chemistry on crosslinkage. Although traditional CS products are affected by the soil chemistry (they may demonstrate a drastic acceleration of gelation), the new CS variants to be used in the demonstration (made to LBNL's specifications) alleviate the problem.

The site of the field demonstration is described in Section 4. The test site is located in central California on the property of the Los Banos Gravel Company, and has a subsurface geology very similar to that at the Hanford reservation. This section covers the geological, physical and geochemical characterization of the site. It also discusses the geochemical characteristics of the soil types, and how their variability may affect the adaptation of the design of the subsurface containment system to the site conditions.

In Section 5 we investigate numerically the emplacement and performance of a barrier system underneath a leaking tank. The scenarios we investigated were consistent with a leaking underground storage tank at the Hanford reservation (the initial target of the subsurface containment technology) in a deep unsaturated formation dominated by sands and gravels. Several sets of simulation runs were conducted, and the effects of varying a number of design and operational parameters were investigated. In this section, however, we present simulation runs obtained when using the optimum set of design parameters which meet field feasibility criteria. These simulations demonstrate that the viscous barrier technology is effective in reducing permeabilities to near-zero levels (10^{-8} cm/sec or less) in very heterogeneous media and in containing contamination within a defined isolation volume.

Section 6 presents the engineering design of the medium-scale field demonstration. Specifications for the injection and monitoring aspects of the field test are set, and engineering drawings for a number of alternatives are provided.

8. ACKNOWLEDGEMENTS

This work was supported by the U.S. Department of Energy, Office of Environmental Management, Office of Technology Development, under Contract No. DE-AC03-76SF00098.

Thanks are due to Mr. Gordon Mills, General Manager of the Los Banos Gravel Company, for his generous help in locating an appropriate site for the field test. Ms. Andrea Hart of MSE (Butte, Montana) is thanked for her support of the project and for her help in keeping this effort adequately funded in Fiscal Year 1995. Drs. C. Oldenburg and Y. Tsang are thanked for their helpful review comments.

8. Acknowledgements

9. REFERENCES

A.P.H.A. *Standard Methods for the Examination of Water and Wastewater*, 16th Edition, American Public Health Association, Washington, DC, 33–34, 1985.

Dagan, G., *Flow and Transport in Porous Formations*, Springer-Verlag, Berlin, 1989.

Finsterle, S., G.J. Moridis, K. Pruess, and P. Persoff, Physical barriers formed from gelling liquids: 1. Numerical design of laboratory and field experiments, *Rep. LBL-35113*, Lawrence Berkeley Laboratory, Berkeley, CA, 1994a.

Finsterle, S., G.J. Moridis, and K. Pruess, A TOUGH2 Equation-of-state module for the simulation of two-phase flow of air, water, and a miscible gelling liquid, *Rep. LBL--36086*, Lawrence Berkeley Laboratory, Berkeley, CA, 1994b.

Garbesi, K., Toward resolving model-measurement discrepancies of radon entry into houses, *Rep. LBL-34244*, Lawrence Berkeley Laboratory, Berkeley, CA, 1994.

Gile, L.H., and R. B. Grossman, *The Desert Soil Project Monograph*, U.S. Department of Agriculture, Soil Conservation Service, 1979.

Kitanidis, P.K., D.L. Freyberg, N. Chan, S. Itagaki, S-I Lee, and A. Dudek-Ronan, *Applications Handbook for FASTCHEM™, Volume 1: Flow Modules*, Electric Power Research Institute, EPRI TR-101218, 1991.

Krupka, K.M., L.E. Eary, J.R. Morrey, R.L. Schmidt, and J.M. Zachara, *Thermochemical Data used by the FASTCHEM™ Package*, Electric Power Research Institute, EPRI EA-5872, 1988.

Lettis, W.R., Late cenozoic stratigraphy and structure of the western margin of the central San Joaquin Valley, California, *U.S. Geological Survey Open File Report 82-526*, 204, 1982.

Luckner, L., M. Th. van Genuchten, and D. Nielsen, A consistent set of parametric models for the two-phase flow of immiscible fluids in the subsurface, *Water Resour. Res.*, *25* (10), 2187-2193, 1989.

Mattigod, S. V., and G. Sposito, Improved method for estimating the standard free energies of formation of smectites, *Geochim. et Cosmochim. Acta*, 45, 1753–1762, 1978.

Moridis, G.J., P. Persoff, H.-Y. Holman, S.J. Muller, K. Pruess, and C.J. Radke, New barrier fluids for containment of contaminants, *Rep. LBL-34673,* Lawrence Berkeley Laboratory, Berkeley, CA, 1993, in *Proceedings of ER '93 Environmental Remediation Conference*, October 24-28, Augusta GA, 941-948, 1993.

Moridis, G.J., P. Persoff, H.-Y. Holman, S. J. Muller, K. Pruess, P. Witherspoon, and C. J. Radke, Containment of contaminants through physical barriers formed from viscous liquids emplaced under controlled viscosity conditions, FY 1993 Annual Report, *Rep. LBL-35114*, Lawrence Berkeley Laboratory, Berkeley, CA, 1994.

Moridis, G.J., L. Myer, P. Persoff, S. Finsterle, J.A. Apps, D. Vasco, S. Muller, P. Yen, P. Williams, B. Freifeld, and K. Pruess, First-level field demonstration of subsurface barrier technology using viscous liquids, *Rep. LBL-37520,* Lawrence Berkeley Laboratory, Berkeley, CA, 1995a.

Moridis, G.J., P. Persoff, J.A. Apps, L. Myer, K. Pruess, and P. Yen, A field test of permeation grouting in heterogeneous soils using a new generation of barrier liquids, *Rep. LBL-37554*, Lawrence Berkeley Laboratory, Berkeley, CA, 1995b.

Moridis, G.J., K. Nihei, K.-H. Lee, W. Frangos, D. Hopkins, C. Garbesi, S. Finsterle, D. Vasco, and K. Pruess, Technologies for subsurface barrier monitoring and verification, *Rep. LBL-38917*, Lawrence Berkeley Laboratory, Berkeley, CA, 1996.

Morrey, J. R., *FASTCHEM™ Package, Volume 4: User's Guide to the ECHEM Equilibrium Geochemistry Code*, Electric Power Research Institute, EPRI EA-5870-CCM, 1988..

Narasimhan, T. N., J.A. Apps, M. Zhu and T.J. Vogele, *Applications Handbook for FASTCHEM™, Volume 2: Chemical Transport Modules,* Electric Power Research Institute, EPRI TR-101218, 1992.

Persoff, P., J. Apps, G.J. Moridis, and K. Pruess, Barriers formed from gelling liquids: Gel-time control for colloidal silica injected into calcareous soils, EOS, Transactions of the American Geophysical Union, 1994 Fall Meeting Supplement, 75(44): 220, (*Rep. LBL -36568*) presented at the Fall 94 American Geophysical Union Meeting, December 5-9, San Francisco, California, 1994a.

Persoff, P., G. J. Moridis, J. Apps, ,K. Pruess, K., and S. J. Muller, Designing injectable colloidal silica barriers for waste isolation at the hanford site, *Rep. LBL-35447*, Lawrence Berkeley Laboratory, Berkeley, CA, 1995, in *In-Situ Remediation: Scientific Basis for*

Current and Future Technologies, 33rd Hanford Symposium on Health and the Environment, November 7-11, 1994, Gee, G.W. and N.R. Wing, eds., Battelle Press, Richland, WA, 87-101, 1994b.

Persoff, P., S. Finsterle, G.J. Moridis, J. Apps, K. Pruess, and S. Muller, Injectable barriers for waste isolation, *Rep. LBL-36884*, Lawrence Berkeley Laboratory, Berkeley, CA, 1995, in ASME/AIChE National Heat Transfer Conference, Portland, Oregon, Aug. 5-9, 1995, *AIChE Symposium Series, 91*(306), 58-67, 1995.

Pruess, K, TOUGH User's Guide, *Rep. LBL-20700*, Lawrence Berkeley Laboratory, Berkeley, CA, 1987.

Pruess, K, TOUGH2 - A general-purpose numerical simulator for multiphase fluid and heat flow, *Rep. LBL-29400*, Lawrence Berkeley Laboratory, Berkeley, CA, 1991.

Reed, M.H. and N. F. Spycher, *CHILLER*, Department of Geological Sciences, University of Oregon, Eugene, Oregon, 1989.

Rockhold, M. L., M. J. Fayer, and P. R. Heller, Physical and hydraulic properties of sediments and engineered materials associated with grouted double-shell tank waste disposal at Hanford, *PNL-XXXX*, UC-510 Draft Report, 1993.

Sposito, G., The polymer model of thermochemical clay mineral stability, *Clays and Clay Minerals*, 34, 198–203, 1986.

Vanselow, A. P., Equilibria of the base exchange reactions of bentonites, permutites, soil colloids and zeolites, *Soil Science*, 33, 95–113, 1932.

Wolery, T. J. and S. A. Daveler, EQ6, A Computer code for reaction-path modeling of aqueous geochemical systems (Version 7): Theoretical manual, user's guide and related documentation, *Lawrence Livermore National Laboratory UCRL-MA-110662-PT-IV*, Livermore, CA, 1992.

Wolery, T.J., EQ3/6, A software package for geochemical modeling of aqueous systems: Package overview and installation guide (Version 7.0), *Lawrence Livermore National Laboratory UCRL-MA-110662-PT-I*, Livermore, CA, 1992.

Yeh, G.-T. and V.S. Tripathi, HYDROGEOCHEM: A Coupled model of hydrogeological and geochemical equilibrium of multicomponent systems, *Oak Ridge National Laboratory ORNL-6371*, Oakridge, TN, 1990.

Yeh, G.-T. and V.S. Tripathi, A model for simulating transport of reactive multispecies components: model development and demonstration, *Water Resour. Res., 27*(11), 3075-3094, 1991.